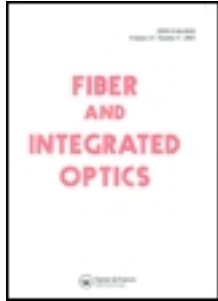


This article was downloaded by: [Universidad Del Pais Vasco]

On: 01 March 2013, At: 08:58

Publisher: Taylor & Francis

Informa Ltd Registered in England and Wales Registered Number: 1072954 Registered office: Mortimer House, 37-41 Mortimer Street, London W1T 3JH, UK



## Fiber and Integrated Optics

Publication details, including instructions for authors and subscription information:

<http://www.tandfonline.com/loi/ufio20>

### Geometric Optics Analysis of Multi-Step Index Optical Fibers

JOSEBA ZUBIA <sup>a</sup>, GOTZON ALDABALDETRERU <sup>b</sup>, GAIZKA DURANA <sup>c</sup>, JON ARRUE <sup>d</sup>,  
CHRISTIAN-ALEXANDER BUNGE <sup>e</sup> & HANS POISEL <sup>f</sup>

<sup>a</sup> Departamento de Electronica y Telecomunicaciones, Universidad del Pais Vasco, Euskal-Herriko Unibertsitatea, Bilbao, Spain

<sup>b</sup> Departamento de Electronica y Telecomunicaciones, Universidad del Pais Vasco, Euskal-Herriko Unibertsitatea, Bilbao, Spain

<sup>c</sup> Departamento de Electronica y Telecomunicaciones, Universidad del Pais Vasco, Euskal-Herriko Unibertsitatea, Bilbao, Spain

<sup>d</sup> Departamento de Electronica y Telecomunicaciones, Universidad del Pais Vasco, Euskal-Herriko Unibertsitatea, Bilbao, Spain

<sup>e</sup> POF-AC, University of Applied Sciences, Nuremberg, Germany

<sup>f</sup> POF-AC, University of Applied Sciences, Nuremberg, Germany

Version of record first published: 24 Jun 2010.

To cite this article: JOSEBA ZUBIA, GOTZON ALDABALDETRERU, GAIZKA DURANA, JON ARRUE, CHRISTIAN-ALEXANDER BUNGE & HANS POISEL (2004): Geometric Optics Analysis of Multi-Step Index Optical Fibers, Fiber and Integrated Optics, 23:2-3, 121-156

To link to this article: <http://dx.doi.org/10.1080/01468030490269080>

PLEASE SCROLL DOWN FOR ARTICLE

Full terms and conditions of use: <http://www.tandfonline.com/page/terms-and-conditions>

This article may be used for research, teaching, and private study purposes. Any substantial or systematic reproduction, redistribution, reselling, loan, sub-licensing, systematic supply, or distribution in any form to anyone is expressly forbidden.

The publisher does not give any warranty express or implied or make any representation that the contents will be complete or accurate or up to date. The accuracy of any instructions, formulae, and drug doses should be independently verified with primary sources. The publisher shall not be liable for any loss, actions, claims, proceedings, demand, or costs or damages whatsoever or howsoever caused arising directly or indirectly in connection with or arising out of the use of this material.

## Geometric Optics Analysis of Multi-Step Index Optical Fibers

JOSEBA ZUBIA  
 GOTZON ALDABALDETRERU  
 GAIZKA DURANA  
 JON ARRUE

Departamento de Electrónica y Telecomunicaciones  
 Universidad del País Vasco  
 Euskal-Herriko Unibertsitatea  
 Bilbao, Spain

CHRISTIAN-ALEXANDER BUNGE  
 HANS POISEL

POF-AC  
 University of Applied Sciences  
 Nuremberg, Germany

*The double aim of the present article is to give a brief description of our research group's main results achieved in recent years and to provide a comprehensive analysis of light propagation properties in multi-step index (MSI) fibers based on the geometric optics method. Therefore, in the initial part we present our research team and its main lines of research on plastic optical fibers (POF). Afterward, the discussion focuses on a new theory we have developed for the propagation in MSI fibers. First of all, we derive the ray invariants  $\tilde{\beta}$  and  $\tilde{l}$ , which allow us to instantly determine the direction of the ray at any position along its trajectory, and we discuss the characteristics of the ray path, setting the classification of rays into bound, refracting and tunneling categories. Then, we calculate the ray-path parameters, namely the path length  $L_p$ , the ray half period  $z_p$  and the ray transit time  $t$ . Furthermore, we analyze the ray temporal dispersion. Specifically, we take a practical case in which the width of each layer is maintained constant, allowing, in contrast, for the respective refractive indices to take any value, and we derive closed expressions for the ray dispersion. Finally, we investigate the light power acceptance properties of an MSI fiber, calculating the effectiveness of both diffuse and collimated light sources in launching bound rays and the coupling losses with lateral and longitudinal misalignments.*

**Keywords** plastic optical fibers, MSI fibers, geometric optics, time dispersion

Received 18 September 2003; accepted 18 September 2003.

The authors thank the Universidad del País Vasco–Euskal Herriko Unibertsitatea and the Ministerio de Ciencia y Tecnología under projects 9/UPV 00147.345-14626/2002ZUBIA and TIC2000-059, respectively, for their financial support.

Address correspondence to Joseba Zubia, Departamento de Electrónica y Telecomunicaciones, Universidad del País Vasco, Euskal-Herriko Unibertsitatea, ETSI de Bilbao, Alda. de Urquijo s/n, Bilbao 48013, Spain. E-mail: jtpuzaj@bi.ehu.es

## Introduction

### *Our Research Team*

The world of fiber optics has attracted a lot of attention since its discovery as a transmission medium in the sixties. Although at the beginning most of the studies were focused on conventional glass optical fibers, in the eighties plastic optical fibers (POF) were already transparent enough to be used as a telecommunications medium. Since then, many researchers have been devoted to the study of properties of POF, although some minor aspects still require a systematic study.

Our research team came into being in 1993 at the Telecommunications Department of the University of the Basque Country, with the express initial purpose of optimizing the transmission distance in communications links through POF. The motivation was that they presented some great advantages over their glass counterparts, although they were only used for distances below 100 m because of their much higher attenuation. This first work led to the interesting conclusion that the use of inexpensive green Light Emitting Diodes (LEDs) instead of the conventional red ones permitted much longer transmission distances, as was theoretically and experimentally demonstrated. Since then, our team has investigated a great variety of topics about POF, and the resultant insight has helped us to develop theoretical and computational models that can predict their transmission properties, including the effect of bends, structural imperfections, and possible stresses to which they may be subjected. Besides, we have designed and tested new active and passive devices based on them, including couplers, modulators, mode scramblers, and several types of sensors, such as seismographs, wind-speed sensors, refractometers, chemical sensors, and so forth.

Currently, an important part of our research is focused on computational analysis of mode mixing, attenuation, bandwidth, and some other parameters that determine the performance of POF optical links, allowing for bends of any shape in our simulations. In addition to step-index POF, graded-index and multi-step index POF are also being studied. On the other hand, we have carried out experimental measurements to check the behavior of light polarization through POF and the influence of several parameters affecting the performance of mode scramblers, and we are adjusting our models of light propagation in real fibers from experimental measurements of the output power distributions with fibers of different lengths. Currently, our team carries out research projects in collaboration with several universities and companies. There are five of us in the group in Bilbao, combining this work with lectures to engineering students, a few of whom become temporary collaborators with us during their elaboration of the project they have to do as the final part of the degree.

### *Plastic Optical Fibers*

Plastic optical fibers using a polymethyl methacrylate (PMMA) core were first introduced in the late sixties, although their initial attenuation was 500 dB/km at 650 nm; that is, too high to result of interest for telecommunications purposes [1]. Figure 1 shows the structure of a typical POF. However, their transparency has improved very much since then, owing to more elaborated manufacturing techniques and, in the case of perfluorinated (PF) POF, to the significant reduction in the CH vibrational absorption that is achieved by replacing hydrogen by a more massive atom, such as fluorine [2]. On the other hand, the transmission rates of POF data links have also been steadily increasing. This is mainly

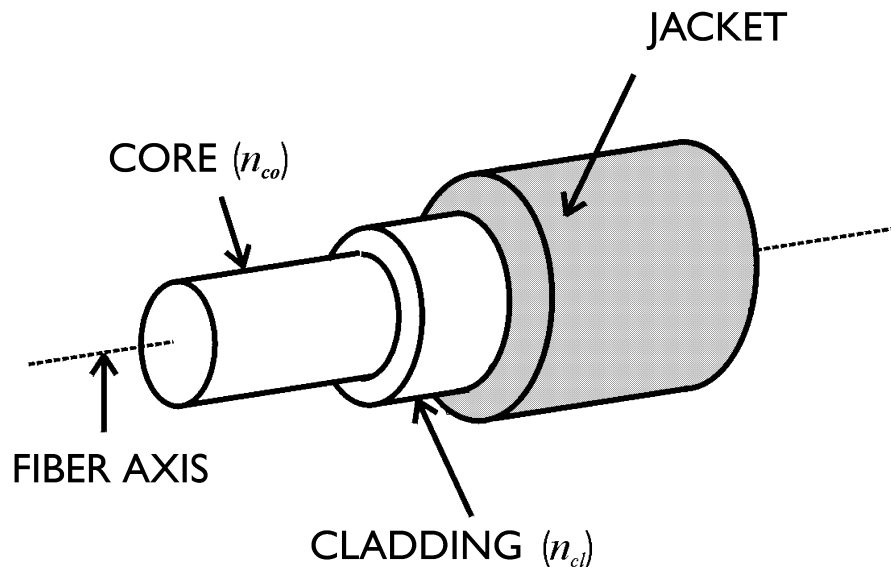


**Figure 1.** Structure of a POF. In a typical SI POF the core diameter is  $980 \mu\text{m}$  and the cladding width  $20 \mu\text{m}$ , the refractive index  $n$  being 1.492 in the core and a lower value in the cladding ranging between 1.40 and 1.42. In a typical perfluorinated GI POF  $n$  decreases from about 1.354 to 1.342 in a core of 120 or 130  $\mu\text{m}$  of diameter, yielding an NA of 0.18 at the center of the core. The refractive index profile exponent is close to 2.

due to the development of novel types of POF, such as graded-index (GI) [3, 4]. Currently, step-index (SI) POF with low numerical aperture (NA) (0.32) matched to low-NA LEDs are commercially available with a typical bandwidth length product of about  $15 \text{ MHz} \cdot \text{km}$  and an attenuation on the order of  $120 \text{ dB/km}$  at  $650 \text{ nm}$  [5]. Much higher bandwidths and distances have been reported with PF GI POF, such as the presently commercially available Lucina fiber ( $1006 \text{ m}$  at  $1.25 \text{ Gbit/s}$  at the wavelength of  $1300 \text{ nm}$ ) [6].

A problem with GI-POF arises when they are curved with very small bend radii, since then bending losses will be much higher than in the case of SI POF, due to both their low numerical aperture at the center of the core (0.18) and the decrease of this value down to zero as we approach the core-cladding interface. This is illustrated in Figure 2, which shows the dependence of bending losses on both the bend radius and the refractive index profile exponent for a typical GI-POF. However, a new type of POF that has already been thought of, namely the multi-step index (MSI) POF [7, 8], can yield a very high bandwidth and yet present a relatively small radiation losses in bends. A theory specially adapted to describe light propagation through MSI POF is developed in this article for the first time. We include a summary of some of the results that we have obtained during the last few years.

### Backward Glance at Our Research in the Last Few Years

Our main lines of research may be classified into three categories: theoretical and computational modeling of POF, active and passive optical devices for POF, and sensors based on POF.

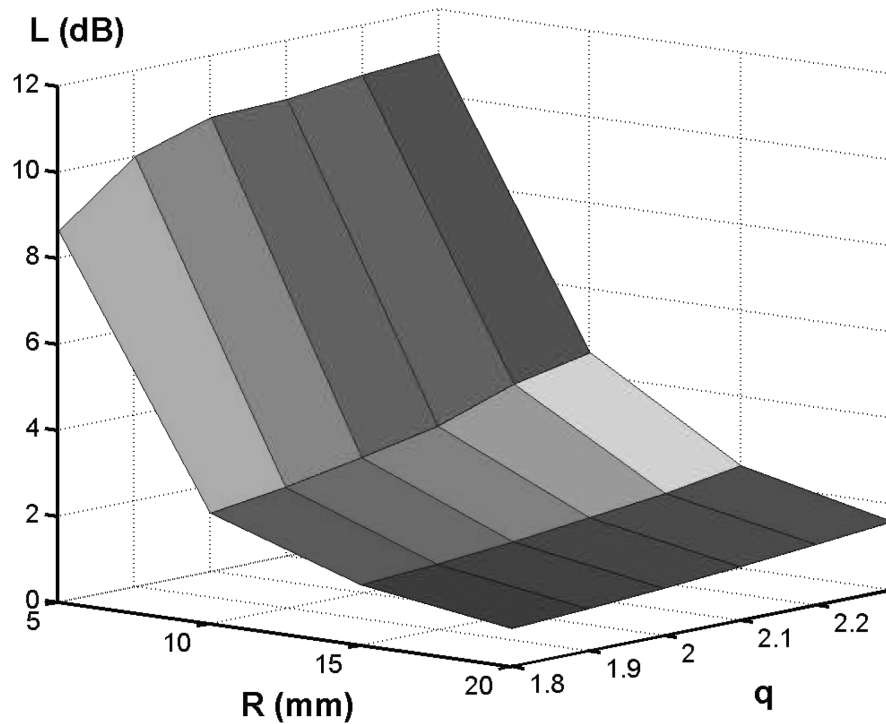


**Figure 2.** Dependence of bending losses on both the bend radius and the refractive index profile exponent for a typical GI-POF. This figure corresponds to a core diameter of  $130\ \mu\text{m}$  and core and cladding refractive indices equal to 1.353 and 1.340, respectively, for half a circular turn.

### *Theoretical and Computational Modeling of POF*

In this section we briefly describe the results we have achieved in relation to light propagation in POF. We started with an overall analysis of light source, POF, and photodiode. Specifically, we analyzed the variations in the photocurrent due to changes in the LED temperature, output power, spectrum width, and spectrum center, in combination with the optical fiber spectral attenuation and length and the photodiode responsivity. With this work, we showed in what way the optimum LED center wavelength varied as a function of the LED spectrum width and the transmission distance. Maximum distances greater than 200 m could be achieved with green LEDs [9].

Afterward, we studied the influence of bends in the link. First, we investigated the influence of the shape of bends on the total radiation loss along two of the most common types of SI POF, as well as the effect produced by variations in the light wavelength. We showed that a circle arc can cause slightly higher attenuation than an ellipse close to it, depending on the refractive indices, but that curves with very sharp sections always introduce higher losses. Even so, we concluded that the easiest curve to achieve, yet one of the best, is the circular one [10]. Recently, we have also proved that a simple circular bend of the appropriate radius placed at the receiver end can improve bandwidth in high-NA POF, depending on the POF length and on the degree of mode mixing along the fiber, and also on the type of light source employed. For example, our results so far seem to confirm Maruo et al.'s [11], who showed that, with a 6.4-mm radius,

360° bend placed in a 100-m long 0.5-NA POF link at a distance  $L$  from a 0.1-NA light source, the maximum improvement is reached for a bending position of  $L = 50\text{--}75$  m. On the other hand, we have also calculated bending losses in GI POF by developing a computer program to simulate POF of any refractive index profile in the proximity of the parabolic one, and also different light wavelengths. We showed that variations in the light wavelength affect total radiation losses because of the presence of tunneling rays, although the corrections due to this effect are small, especially when the fiber diameter is large [12]. We also studied the influence of the cladding thickness on optical losses when SI POF are bent. The most interesting conclusion was that, for large bend radii, bending losses are approximately independent of cladding thickness. However, the assumption of infinite cladding thickness is reached for a cladding thickness of about 4 mm for 1-mm core POF. This implies a difference of 2 dB between real POF (finite cladding and lower losses) and an ideal one (infinite cladding). This data corresponds to fiber turns with a bend radius of 8 mm [13].

We also investigated the photoelastic effects in POF. Specifically, we analyzed the optical effects induced by three different types of stresses. We saw that a uniaxial stress makes an isotropic POF uniaxial, with its optic axis parallel to the fiber axis. On the other hand, bending and torsion stresses convert the fiber into an inhomogeneous medium, because the refractive index depends on the position as well as on the direction of the ray path through the POF. However, we showed that these stresses have no noticeable effect on the modal dispersion in SI POF. The corrections were less than one-hundredth of its original value in all cases [14, 15].

Besides, we analyzed the relationship between the depolarization of the light along the POF and the quality of the fiber. We saw that the core-cladding interface quality is one of the most important parameters that influences the light polarization state of a wave traveling along a POF, which was successfully tested empirically [16]. To give a quantitative account of the mode-coupling rate as a consequence of fiber impurities and inhomogeneities, we developed a new and simple method that only requires the observation of the far-field output pattern for different launching angles over a fixed length of fiber [17, 18]. This method is based on Gloge's flow equation.

Currently, we can simulate the influence of fiber impurities on temporal dispersion of pulses and other transmission parameters by means of a computer program based on shifts in the propagation direction of light rays every certain distance, which we have called "mean free path," and according to a random Gaussian deviation that has been adjusted experimentally for a typical SI POF [19]. This software tool is able to model real fibers.

### ***Active and Passive Optical Devices for POF***

By means of both computer simulations and experimental measurements we have designed mode scramblers, active and passive couplers, and optical switches for POF. The procedure for mode scrambling involves curving the POF inward and outward repeatedly, with the appropriate bend radii and lengths of the straight and bent sections for the type of POF considered [20–24]. We have seen that the purpose of approaching the equilibrium mode distribution in SI and GI POF can be achieved with various different setups, consisting of two or more cylinders around which the POF is bent. In the case of the eight-shaped configuration, the appropriate radius of the cylinders can vary from 10 to 21 millimeters. For example, two complete turns with a radius of 10 millimeters and a separation between the centers of the mandrels of 30 millimeters can work for standard high-NA PMMA POF, a greater radii up to 21 millimeters can serve as well if

we increase significantly the number of complete turns. The distance between the centers of the cylinders can be varied from 30 to 120 millimeters for fine-tuning, but it does not affect the performance if it is longer. For standard GI POF the main difference is that larger bend radii are needed (18–20 millimeters). We have also seen that the redistribution of power along the bends mainly occurs at the initial part of the bend (the first quarter of circular turn is more influential than the second one), so prolonging the arc lengths is nearly irrelevant from a certain minimum length (1/2 turn and 1 turn yield very similar results), although too short a bent section also has little influence on the final result of the scrambler, as has been checked experimentally by eliminating the first and last short bent sections in eight-shaped scramblers, such as in the setup mentioned above for a high-NA PMMA POF. Similarly, the length of the straight sections between consecutive bends have proved to be influential in the final result, but only when these are not too long, as can be deduced from our results for different separations between the cylinders. For example, we have checked for SI POF that there is no significant difference between the distance of about 120 millimeters and a distance of 240 millimeters.

On the other hand, we have previously pointed out that the shape in which the fiber is bent determines its attenuation. From this conclusion, we had the idea of designing POF couplers whose coupling ratio could be controlled by changing the curvature of two fibers whose cores were partially polished and in contact with each other along a short section. We found that the most relevant factor that determined the coupling ratio was the polishing depth. An equal power splitting ratio can be obtained, for instance, with a null separation between the fiber axes and a coupling length of 35 mm [25]. Active couplers and switches were achieved by placing a liquid crystal (LC) between the two fibers [26, 27]. The LC chosen had parallel and perpendicular refractive indices of 1.5342 and 1.4717 respectively, and excess losses were about 3 dB.

### ***Sensors Based on POF***

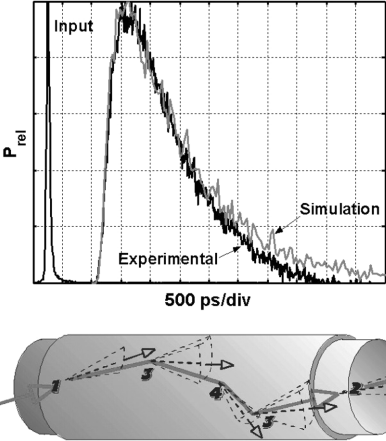
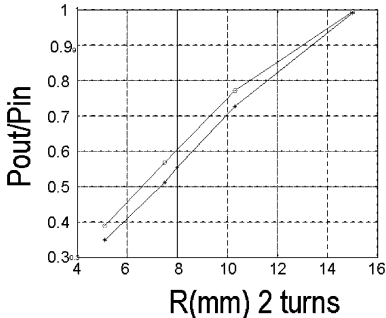
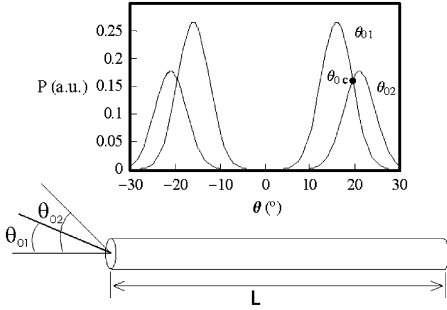
Some of the sensors developed by us and Professor Lopez-Higuera's group were based on power variations of the light launched from one fiber to another, both with the fibers aligned in the same direction and in opposite directions, with a reflecting surface in front of them. In some cases, a rotating device that interrupted the transmission of light periodically was placed in the way from one fiber to the other one, thus allowing us to measure parameters such as wind speed [28]. In other sensors, it was the variations in the transmitted light due to different refractive indices of the medium that determined the value of the parameter to be measured; for example, the concentration of an acid [29]. On the other hand, a single fiber was sometimes employed to measure parameters such as the refractive index of the outer medium or shifts in the position of the end of the fiber, as in our seismograph. In the former case, the fiber was uncladded and curved in the shape of several turns. It was able to measure refractive indices in the range between 1.33 and 1.44 [21, 30].

Our research results are graphically summarized in Tables 1 through 3.

### **Multi-Step Index Fibers**

Multi-step index (MSI) fibers constitute a serious alternative to graded index (GI) fibers, and especially to GI polymer optical fibers (GI-POF) [7, 8]. This is due to the simpler processes involved in the manufacturing of these types of fibers, as well as to the stability of their index profiles with aging and with temperature and humidity changes.

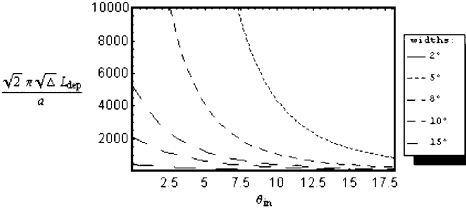
**Table 1**  
Theoretical and computational modeling of POF

Characteristics	Results
<p>A comprehensive software package capable of modeling real POF is being developed. It includes bulk and surface scattering and is based on both the ray tracing and the WKB methods. It yields dispersion, attenuation, far and near fields, connector losses, and so on. The top figure shows that the predicted dispersion matches the experimental one. The lower figure represents the essential idea in our model.</p>	
<p>Bending loss calculations interested us from the beginning. From ray tracing models in POF, we can calculate bending loss as a function of the ratio of bend radius to fiber core radius, for any refractive index profile and including the wavelength dependence through tunneling rays. Typical bending losses are exemplified in the figure, in which we show the results for two full turns in a 1 mm diameter PMMA SI POF as a function of the radius of curvature, both considering (upper curve) and neglecting (lower curve) tunneling rays. These results are very important to design mode scramblers.</p>	
<p>A new method for measuring mode coupling in highly multimode SI POF was developed. It consists in launching two collimated beams at two different angles, as this figure shows. By measuring the intersection points of the respective far-field curves, the mode conversion coefficients can be easily deduced. The main advantage of our method is that it is not necessary to cut the fiber, maintaining unchanged the setup conditions during the whole experiment.</p>	

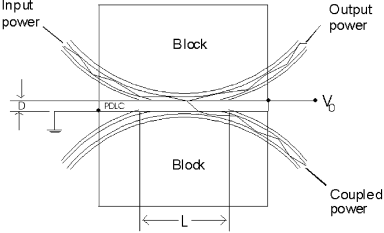
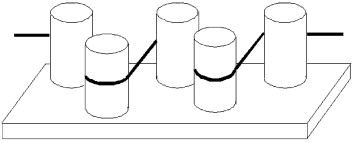
(continued)



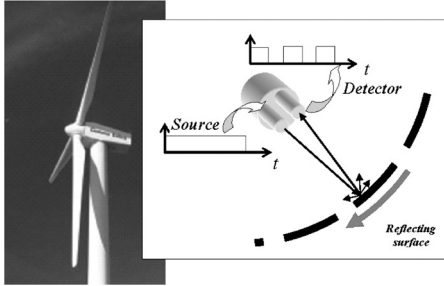
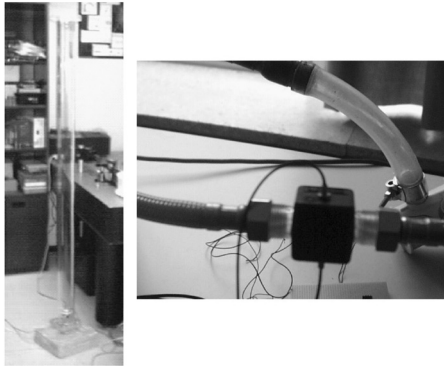
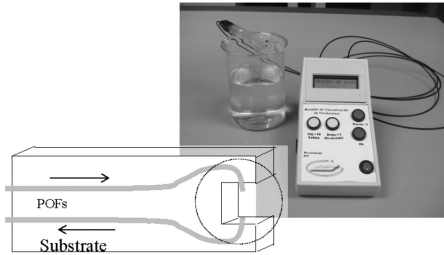
**Table 1**  
(Continued)

Characteristics	Results
<p>One open question is the behavior of the polarization state as the light travels along a POF. Different kinds of studies have been carried out for short POF sections, including the effect of wavelength, refractive indices, diameter, and light launching conditions. For example, we have found a noticeable dependence of the output degree of polarization on the light-launching angle, which has been presented in the frame of a theoretical model. These studies are focused on testing, if possible, the quality of the core-cladding interface through polarization measurements.</p>	 <p>The graph plots the normalized polarization parameter <math>\frac{\sqrt{2} \pi \sqrt{\Delta} i_{dep}}{a}</math> on the y-axis (ranging from 0 to 10000) against the light-launching angle <math>\theta_{in}</math> on the x-axis (ranging from 0 to 17.5 degrees). Five curves are shown for different fiber diameters: 2°, 5°, 8°, 10°, and 15°. The curves show that the polarization parameter increases significantly with the light-launching angle, and the rate of increase is higher for larger diameters.</p>

**Table 2**  
Active and passive optical devices for POF

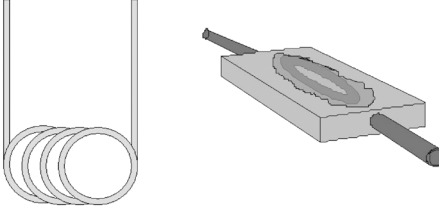
Characteristics	Device
<p>Active coupler and switch. By introducing a liquid crystal (LC) between two partially polished POF we can control the amount of power exiting the output ports. The coupling rate can be varied in 5 dB by applying a low voltage to the LC layer inserted between the fibers. We have designed two prototypes based on a nematic LC and on a polymer-dispersed one (PDLC), respectively.</p>	 <p>The diagram shows two partially polished POF fibers (represented as curved lines) positioned symmetrically around a central liquid crystal (LC) layer. The LC layer is sandwiched between two rectangular blocks. Input power enters from the left, and output power exits from the right. A voltage <math>V_0</math> is applied across the LC layer. The length of the LC layer is denoted as <math>L</math>. Coupled power is shown exiting from the bottom fiber.</p>
<p>Scramblers. By studying the influence of bends on the far field it is possible to design scramblers for SI and GI POF. This figure shows one of our approaches, where the distance between cylinders may vary in order to get the equilibrium mode distribution. At the same time it is very important to maintain low excess losses (less than 1 dB for some applications).</p>	 <p>The diagram illustrates a POF scrambler consisting of a series of five cylindrical rods of varying heights and positions, through which a POF fiber is bent. The fiber enters from the left and exits to the right after passing through the cylinders, which are mounted on a common base.</p>

**Table 3**  
Sensors based on POF

Characteristics	POF sensor
<p>POF-based wind speed sensor. It consists of two fibers and a rotating device attached to an anemometer. By counting the number of reflected pulses caused by the rotating cylinder, we can calculate the wind speed without any drawback originated by sparks or electric storms. The signal travels toward the bottom of the wind generator, where it is analyzed. In this design we used two SI POF: one for emitting light, and another one for detecting the reflected light.</p>	
<p>A seismograph and a flow sensor constitute two of the prototypes of sensors we are currently working on. The former is based on the light emitted by a 2 m-high POF onto a two-dimensional photodiode array. Any vibration of the ground results in a variation of the recorded light intensity. The other sensor, a flow one, is based on the light modulation generated by a propeller moved by the liquid flow, which blocks the light transmission. The number of transmitted pulses gives us the flow. It is also possible to roughly know the turbidity from the magnitude of the transmitted light.</p>	
<p>This intensity sensor measures concentrations of HF and HCl acids in water. Variations of light intensity serve to deduce acid concentrations. The light power attenuates as it crosses the path between the two end faces of the emitting and receiving POF. The acids are situated between the two fibers.</p>	

(continued)

**Table 3**  
(Continued)

Characteristics	POF sensor
<p>We have designed and measured passive devices based on plastic optical fibers (POF) to determine the index of refraction of liquids. The principle behind the first approach is the light power leakage along tightly bent POF stripped of their cladding. Introducing more than half a turn in the active POF hardly improves the sensor's response. The other design is based on the power lost by a partially polished POF due to the presence of a liquid on the polished side, which causes the appearance of leaky rays.</p>	

Furthermore, MSI fibers allow high bandwidths on the order of  $250 \text{ MHz} \cdot 100 \text{ m}$  when considering, for instance, an MSI POF of three layers with a numerical aperture (NA) of 0.25, which complies with the IEEE1394/S400 specification [8, 32], thus increasing their popularity.

Taking into account that there are many theoretical aspects regarding the performance of MSI fibers missing, we have carried out an extensive analysis of light propagation properties in such fibers using geometric optics; the results will be shown in the following sections.

## Bound Rays in Multi-Step Index Fibers

### Structure of Multi-Step Index Fibers

Figure 3 shows the refractive index profile in a multi-step index fiber of five layers [7], whereas the most general refractive index profile in multi-step index fibers is plotted on Figure 4.

### Ray Paths in Multi-Step Index Fibers

The general equation for a ray path, derived from the Eikonal equation, may be written as follows [31]:

$$\frac{d}{ds} \left( n \frac{d\vec{R}}{ds} \right) = \vec{\nabla} n. \quad (1)$$

Figure 5 shows the meaning of the parameters involved in Equation (1):  $s$  is the distance measured along the path,  $\vec{R}$  is the position vector for a point on the ray path, and  $d\vec{R}/ds$  is a unit vector tangent to the ray path and  $z$  the fiber axis.

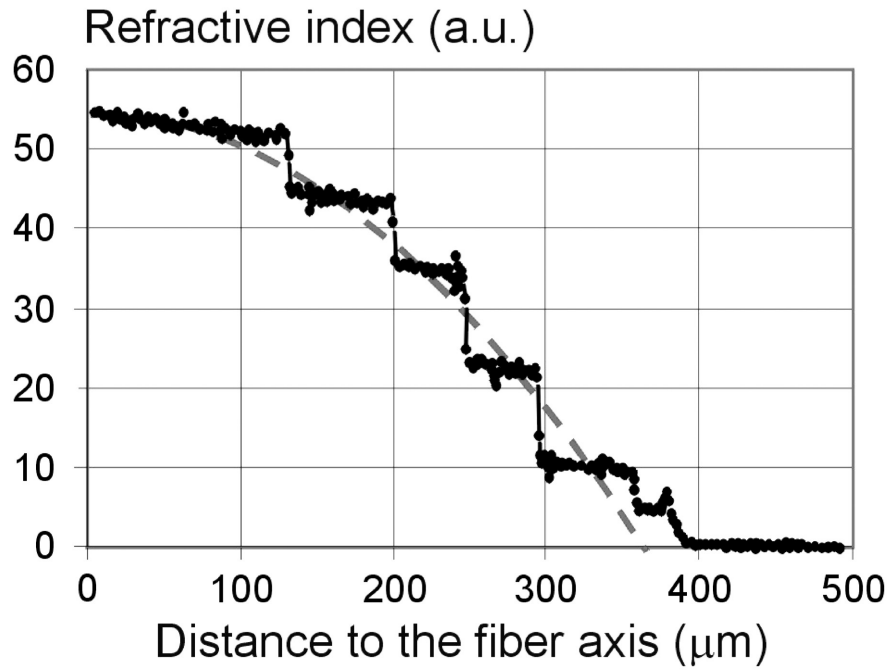


**Figure 3.** Measured refractive index profile for a multi-step index fiber of five layers. This plot is taken from Levin et al. [7].

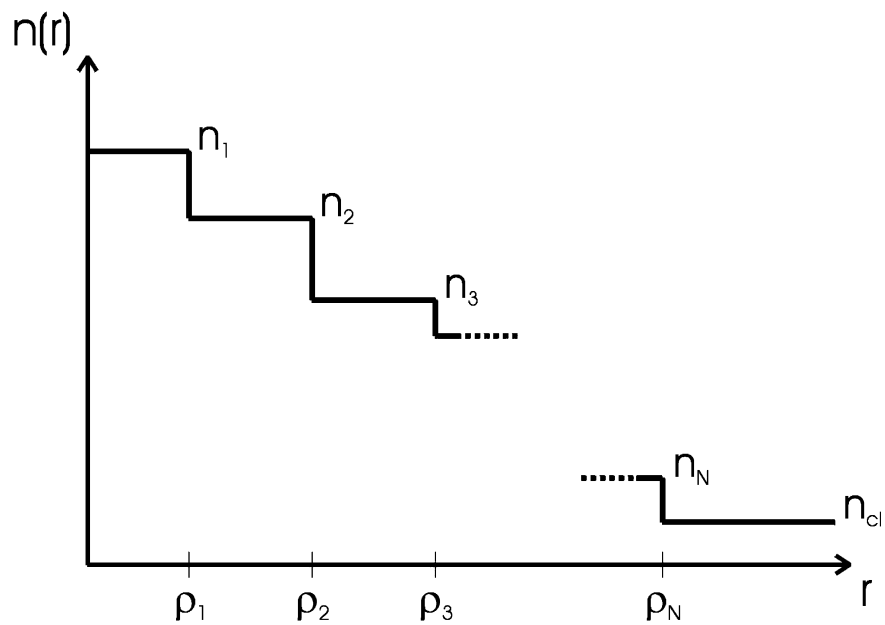


**Figure 4.** Most general refractive index profile in multi-step index fibers.

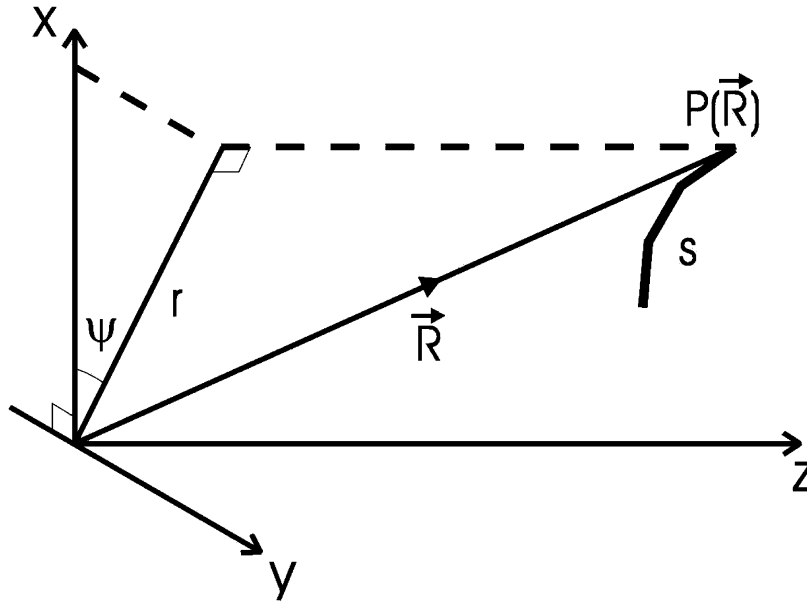


Figure 5. Ray trajectory in multi-step index fibers.

In MSI fibers

$$n(\vec{R}) = \begin{cases} n_1 = n_{co}; & r < \rho_1, \\ n_2; & \rho_1 \leq r < \rho_2, \\ \vdots \\ n_N; & \rho_{N-1} \leq r < \rho_N, \\ n_{cl}; & r \geq \rho_N. \end{cases} \quad (2)$$

We can simplify the above expressions if we consider only MSI fibers of two layers (as shown in Figure 6):

$$n(r) = \begin{cases} n_1; & r < \rho_1, \\ n_2; & \rho_1 \leq r < \rho_2, \\ n_{cl}; & r \geq \rho_2. \end{cases}$$

### Ray Invariants

From Equation (1) we have

$$n \frac{dz}{ds} = \text{constant},$$

and name the angle between the ray path and longitudinal axis  $\theta_z$ ,

$$\frac{dz}{ds} = \cos \theta_z.$$

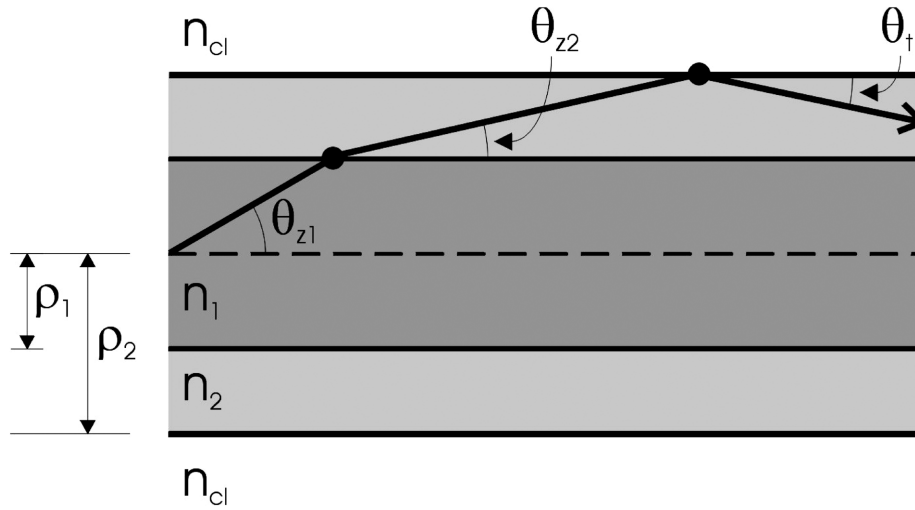


Figure 6. Example of the ray trajectory in an MSI fiber of two layers.

We call the ray invariant  $\tilde{\beta}$ :

$$\tilde{\beta} = n \cos \theta_z = n \frac{dz}{ds} = \begin{cases} n_1 \cos \theta_{z1}; & r < \rho_1, \\ n_2 \cos \theta_{z2}; & \rho_1 \leq r < \rho_2, \\ \vdots \\ n_N \cos \theta_{zN}; & \rho_{N-1} \leq r < \rho_N, \\ n_{cl} \cos \theta_t; & r \geq \rho_N. \end{cases} \quad (3)$$

which is related to the translational invariance of the MSI fiber. In the same way, we define the invariant  $\tilde{l}$  as

$$\tilde{l} = \frac{\rho_i}{\rho_N} n_i \sin \theta_{zi} \cos \theta_{\phi_i}; \quad i = 1 \dots N, \quad (4)$$

which accounts for the azimuthal symmetry of the fiber.

Figure 7 shows the definitions of the angles used above when considering an MSI fiber of two layers:  $\alpha$  is the angle of incidence or reflection relative to the normal PN,  $\theta_z$  is the angle that the incident or reflected ray makes with the axial direction PQ, and  $\theta_\phi$  is the angle the incident or reflected ray makes in the cross section between the tangent at P and the path projection. For meridional rays,  $\theta_{\phi_i} = 0 \Rightarrow \tilde{l} = 0$ .

These two invariants are not independent of each other but they are related by Snell's law:

$$\begin{aligned} \tilde{\beta}^2 + \tilde{l}^2 \frac{\rho_N^2}{\rho_i^2} &= \text{constant}, \\ n_i^2 \cos^2 \theta_{zi} + n_i^2 \sin^2 \theta_{zi} \cos^2 \theta_{\phi_i} &= \text{constant}, \\ n_i^2 \sin^2 \alpha_i &= \text{constant}. \end{aligned}$$

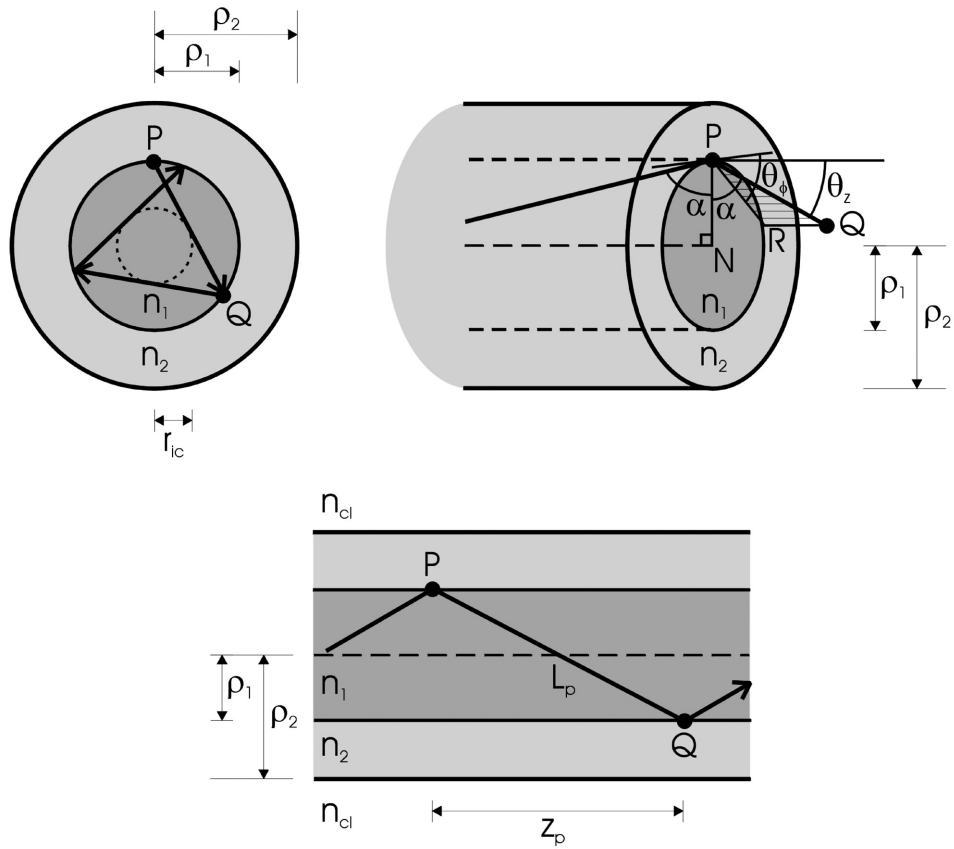


**Figure 7.** Definition of the angles and distances in an MSI fiber of two layers.

### Characteristics of the Ray Path

From the definition of the ray invariants, that is to say, from Equations (3) and (4), the ray path equation yields

$$g(r) = \tilde{\beta}^2 \left( \frac{dr}{dz} \right)^2 = n^2 - \tilde{\beta}^2 - \frac{\tilde{l}^2 \rho_N^2}{r^2} \Big|_{r=\rho_i} \quad (5)$$

A ray propagates when

$$g(r)|_{r=\rho_i} = n^2 - \tilde{\beta}^2 - \frac{\tilde{l}^2 \rho_N^2}{\rho_i^2} > 0$$

thus, a ray has a turning point  $r_{tp} = \rho$  when 1)  $n_i^2 > \tilde{\beta}^2 + \tilde{l}^2 \rho_N^2 / \rho_i^2$  (the ray does propagate within the  $i$ th layer), and 2)  $n_{i+1}^2 < \tilde{\beta}^2 + \tilde{l}^2 \rho_N^2 / \rho_i^2$  (the ray does not continue propagating beyond the  $i$ th layer); that is,

$$n_{i+1}^2 < \tilde{\beta}^2 + \frac{\tilde{l}^2 \rho_N^2}{\rho_i^2} < n_i^2 \Leftrightarrow r_{tp} = \rho_i. \quad (6)$$

Additionally, there is an inner caustic point for skew rays, whose radius  $r_{ic}$  is given by

$$g(r)|_{r=r_{ic}} = 0 \Rightarrow n_i^2 - \tilde{\beta}^2 - \frac{\tilde{l}^2 \rho_N^2}{r_{ic}^2} = 0, \tag{7}$$

$$r_{ic}^2 = \frac{\tilde{l}^2 \rho_N^2}{n_i^2 - \tilde{\beta}^2} = \rho_i^2 \cos^2 \theta_{\phi_i}.$$

For instance, the inner caustic radius  $r_{ic}$  for an MSI fiber of two layers is

$$r_{ic} = \left\{ \begin{array}{l} \rho_1 \cos \theta_{\phi_1} \quad \text{when } r_{tp} = \rho_1 \\ \left( n_2^2 < \tilde{\beta}^2 + \tilde{l}^2 \frac{\rho_2^2}{\rho_1^2} < n_1^2 \right) \\ \left. \begin{array}{l} \left[ \rho_1 \cos \theta_{\phi_1} \quad \text{if } \rho_2 \cos \theta_{\phi_2} < \rho_1, \right. \\ \left[ 0 < \tilde{l}^2 < \frac{\rho_1^2}{\rho_2^2} (n_2^2 - \tilde{\beta}^2) \right] \\ \left. \rho_2 \cos \theta_{\phi_2} \quad \text{if } \rho_2 \cos \theta_{\phi_2} > \rho_1, \right. \\ \left[ n_2^2 - \tilde{\beta}^2 > \tilde{l}^2 > \frac{\rho_1^2}{\rho_2^2} (n_2^2 - \tilde{\beta}^2) \right] \end{array} \right\} \begin{array}{l} \text{when } r_{tp} = \rho_2 \\ (n_{cl}^2 < \tilde{\beta}^2 + \tilde{l}^2 < n_2^2) \end{array}$$

**Classification of Rays**

Taking into account that Equation (5) determines whether rays propagate or not, we can classify rays as follows:

- Bound rays: These rays are bound to the fiber cores and do not leak into the cladding.  $g(r) > 0 \forall r < \rho_N$ .
- Refracting rays: These rays reach the core-cladding interface.  $g(r)|_{r=\rho_N} > 0$ ; that is,  $0 < \tilde{\beta}^2 + \tilde{l}^2 \rho_N^2 / \rho_i^2 < n_{cl}^2$ .
- Tunneling rays: These rays have a turning point ( $r_{tp} = \rho_i$ ) satisfying  $\tilde{\beta}^2 < n_{i+1}^2$  and  $n_{i+1}^2 < \tilde{\beta}^2 + \tilde{l}^2 \rho_N^2 / \rho_i^2$ .

Let us take a practical case in which the width of each layer is maintained constant (i.e.,  $\rho_i - \rho_{i-1} = \text{constant } \forall i$ ) and the refractive indices of the MSI fiber are fitted using two different approaches:

- 1) Linear MSI fiber: The refractive indices of each layer decrease linearly outward.
- 2) Parabolic MSI fiber: The refractive indices of each layer have been calculated in such a way that the overall refractive index profile approximates to the clad parabolic profile.

For a PMMA fiber, the inner layer has a refractive index of  $n_1 = 1.492$ , whereas the cladding refractive index has a value of  $n_{cl} = 1.402$ . The outermost layer has a normalized radius of  $\rho_N = 1$ .

Figure 8 shows several schematic distributions of rays according to the value of the invariants  $\tilde{\beta}$  and  $\tilde{l}$  for  $N = 1, 2,$  and  $6$  layers and for the two different fibers considered



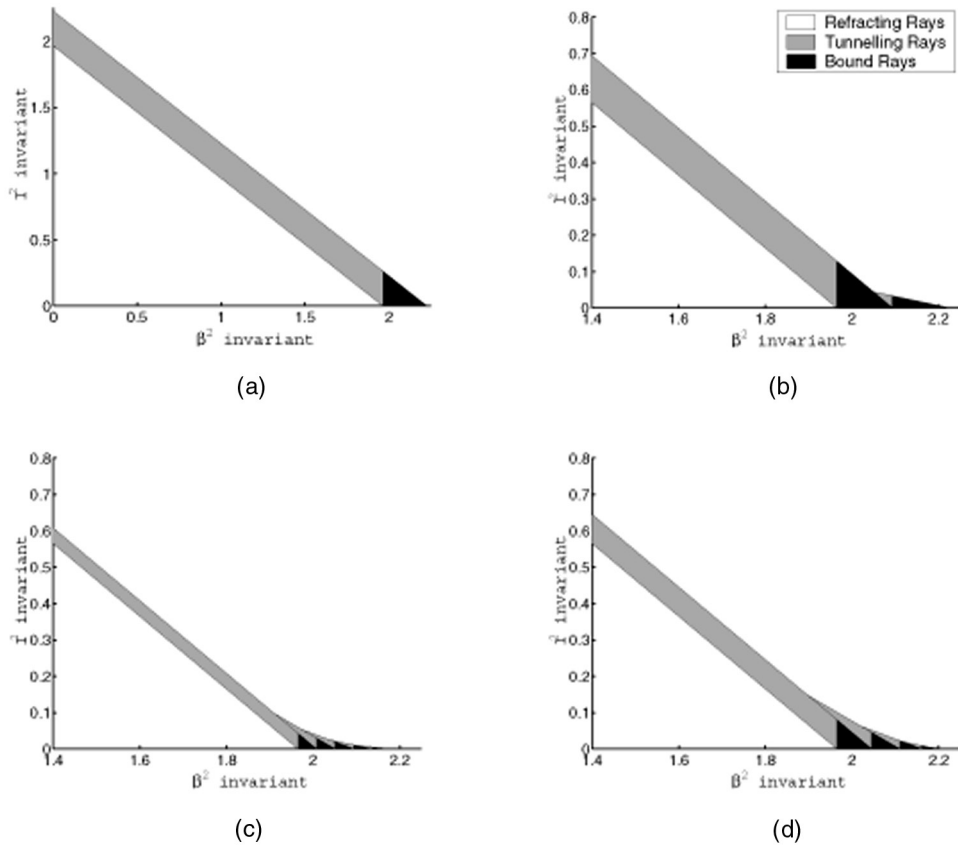


**Figure 8.** Schematic distribution of rays in MSI fibers: a) One-layer linear MSI fiber; b) two-layer linear MSI fiber; c) six-layer linear MSI fiber; d) six-layer parabolic MSI fiber

above (please notice that we have zoomed in so as to have a clearer representation in Figures 8b, 8c, and 8d).

For  $N = 1$  the schematic classification of the rays reduces to that for step-index fibers. It is noticeable that as the number of layers increases, the proportion of the sum of tunneling and bound rays to refracting rays decreases. From Figures 8c and 8d, it can be seen that for the linear MSI fiber, there are less tunneling rays (although the same happens to bound rays), than for parabolic MSI fiber. As the number of layers increases, the range of allowed values of  $\tilde{l}$  for the parabolic MSI fiber tends to that for a clad parabolic profile fiber.

### Ray Path Parameters

We define the local numerical aperture from the complementary critical angle

$$NA_i = \sqrt{n_i^2 - n_{cl}^2}; \quad \rho_{i-1} \leq r \leq \rho_i \quad (8)$$

It can be seen that

$$NA_{i-1} > NA_i.$$

Next, we obtain the new ray trajectory from

$$g(r) = \tilde{\beta}^2 \left( \frac{dr}{dz} \right)^2 \Rightarrow z - z_0 = \tilde{\beta} \int_{r_0}^r \frac{dr}{\sqrt{g(r)}} \quad (9)$$

The path length  $L_p$  is calculated as follows

$$L_p = \int_P^Q ds = 2 \int_{r_{ic}}^{r_{tp}} \frac{n}{\sqrt{g(r)}} dr \quad (10)$$

We can generalize Equation (10) to the N-layer expression

$$L_p = \begin{cases} \text{A when} \begin{cases} n_{i+1}^2 < \tilde{\beta}^2 + \frac{\tilde{l}^2 \rho_N^2}{\rho_i^2} < n_i^2 \\ \rho_{i-1}^2 < \frac{\tilde{l}^2 \rho_N^2}{n_i^2 - \tilde{\beta}^2} < \rho_i^2 \end{cases} & i = 1 \dots N, \\ \text{B when} \begin{cases} n_{y+1}^2 < \tilde{\beta}^2 + \frac{\tilde{l}^2 \rho_N^2}{\rho_y^2} < n_y^2 \\ \rho_{x-1}^2 < \frac{\tilde{l}^2 \rho_N^2}{n_x^2 - \tilde{\beta}^2} < \rho_x^2 \end{cases} & \begin{cases} y = 2 \dots N, \\ x = 1 \dots y - 1, \end{cases} \end{cases} \quad (11)$$

where

$$\begin{aligned} \text{A} &= \frac{2n_i}{n_i^2 - \tilde{\beta}^2} \rho_i \sqrt{n_i^2 - \tilde{\beta}^2 - \frac{\tilde{l}^2 \rho_N^2}{\rho_i^2}} \\ \text{B} &= \frac{2n_x}{n_x^2 - \tilde{\beta}^2} \rho_x \sqrt{n_x^2 - \tilde{\beta}^2 - \frac{\tilde{l}^2 \rho_N^2}{\rho_x^2}} \\ &+ \sum_{i=x+1}^y \left[ \frac{2n_i}{n_i^2 - \tilde{\beta}^2} \left( \rho_i \sqrt{n_i^2 - \tilde{\beta}^2 - \frac{\tilde{l}^2 \rho_N^2}{\rho_i^2}} - \rho_{i-1} \sqrt{n_i^2 - \tilde{\beta}^2 - \frac{\tilde{l}^2 \rho_N^2}{\rho_{i-1}^2}} \right) \right] \end{aligned}$$

and

$$\begin{cases} \rho_0 = 0, \\ n_{N+1} = n_{cl}. \end{cases}$$

Next, we will calculate the ray half-period  $z_p$ , which is defined as the axial distance between successive turning points

$$z_p = \frac{1}{N} = 2\tilde{\beta} \int_{r_{ic}}^{r_{tp}} \frac{1}{\sqrt{g(r)}} dr. \quad (12)$$

Therefore

$$z_p = \begin{cases} \text{C when} & \begin{cases} n_{i+1}^2 < \tilde{\beta}^2 + \frac{\tilde{l}^2 \rho_N^2}{\rho_i^2} < n_i^2 \\ \rho_{i-1}^2 < \frac{\tilde{l}^2 \rho_N^2}{n_i^2 - \tilde{\beta}^2} < \rho_i^2 \end{cases} & i = 1 \dots N \\ \text{D when} & \begin{cases} n_{y+1}^2 < \tilde{\beta}^2 + \frac{\tilde{l}^2 \rho_N^2}{\rho_y^2} < n_y^2 \\ \rho_{x-1}^2 < \frac{\tilde{l}^2 \rho_N^2}{n_x^2 - \tilde{\beta}^2} < \rho_x^2 \end{cases} & \begin{cases} y = 2 \dots N \\ x = 1 \dots y - 1 \end{cases} \end{cases} \quad (13)$$

where

$$\begin{aligned} \text{C} &= \frac{2\tilde{\beta}}{n_i^2 - \tilde{\beta}^2} \rho_i \sqrt{n_i^2 - \tilde{\beta}^2 - \frac{\tilde{l}^2 \rho_N^2}{\rho_i^2}}, \\ \text{D} &= \frac{2\tilde{\beta}}{n_x^2 - \tilde{\beta}^2} \rho_x \sqrt{n_x^2 - \tilde{\beta}^2 - \frac{\tilde{l}^2 \rho_N^2}{\rho_x^2}} \\ &+ \sum_{i=x+1}^y \left[ \frac{2\tilde{\beta}}{n_i^2 - \tilde{\beta}^2} \left( \rho_i \sqrt{n_i^2 - \tilde{\beta}^2 - \frac{\tilde{l}^2 \rho_N^2}{\rho_i^2}} - \rho_{i-1} \sqrt{n_i^2 - \tilde{\beta}^2 - \frac{\tilde{l}^2 \rho_N^2}{\rho_{i-1}^2}} \right) \right]. \end{aligned}$$

### Ray Transit Times in Multi-Step Fibers

The ray transit time is defined as the time taken for a ray to propagate a distance  $z$  along a waveguide, which is given by

$$t = \frac{1}{c} \int n \, ds = \frac{1}{c\tilde{\beta}} \int_0^z n^2 \, dz. \quad (14)$$

Noting the periodicity of the ray path, if we name the point where  $r = r_{ic}$  A and the point where  $r = r_{ip}$  B, then

$$\frac{t}{z} = \frac{t_{AB}}{z_p}$$

By definition, the transit time over a ray half-period  $z_p$  is  $L_0/c$ ; that is,

$$t = \frac{z L_0}{c z_p}.$$

Therefore,

$$t = \begin{cases} \text{E when} & \begin{cases} n_{i+1}^2 < \tilde{\beta}^2 + \frac{\tilde{l}^2 \rho_N^2}{\rho_i^2} < n_i^2 \\ \rho_{i-1}^2 < \frac{\tilde{l}^2 \rho_N^2}{n_i^2 - \tilde{\beta}^2} < \rho_i^2 \end{cases} & i = 1 \dots N, \\ \text{F when} & \begin{cases} n_{y+1}^2 < \tilde{\beta}^2 + \frac{\tilde{l}^2 \rho_N^2}{\rho_y^2} < n_y^2 \\ \rho_{x-1}^2 < \frac{\tilde{l}^2 \rho_N^2}{n_x^2 - \tilde{\beta}^2} < \rho_x^2 \end{cases} & \begin{cases} y = 2 \dots N, \\ x = 1 \dots y - 1, \end{cases} \end{cases} \quad (15)$$

where

$$E = \frac{z}{c\tilde{\beta}} n_i^2$$

$$F = \frac{z}{c\tilde{\beta}} \frac{n_x^2 G + \sum_{i=x+1}^y \left[ \frac{n_i^2}{n_i^2 - \tilde{\beta}^2} \left( \rho_i \sqrt{n_i^2 - \tilde{\beta}^2 - \frac{\tilde{l}^2 \rho_N^2}{\rho_i^2}} - \rho_{i-1} \sqrt{n_i^2 - \tilde{\beta}^2 - \frac{\tilde{l}^2 \rho_N^2}{\rho_{i-1}^2}} \right) \right]}{G + \sum_{i=x+1}^y \left[ \frac{1}{n_i^2 - \tilde{\beta}^2} \left( \rho_i \sqrt{n_i^2 - \tilde{\beta}^2 - \frac{\tilde{l}^2 \rho_N^2}{\rho_i^2}} - \rho_{i-1} \sqrt{n_i^2 - \tilde{\beta}^2 - \frac{\tilde{l}^2 \rho_N^2}{\rho_{i-1}^2}} \right) \right]}$$

$$G = \frac{\rho_x}{n_x^2 - \tilde{\beta}^2} \sqrt{n_x^2 - \tilde{\beta}^2 - \frac{\tilde{l}^2 \rho_N^2}{\rho_x^2}}.$$

In contrast to graded index optical fibers, the dependence of  $t$  on  $\tilde{l}$  is very strong, as the simulations carried out have demonstrated.

Figures 9 and 10 show the ray transit time as a function of the ray invariants  $\tilde{\beta}$  and  $\tilde{l}$  for  $N = 2, 6,$  and  $10$  layers and for the aforementioned two different MSI fibers taking the practical case in which the width of each layer is maintained constant (see previous section on ray classification). Specifically, the ray transit time as a function of  $\tilde{\beta}$  and  $\tilde{l}$  is shown at the top, whereas the ray transit time considering only meridional rays ( $\tilde{l} = 0$ ) is drawn at the bottom (it turns out to be the rear projection of the ray transit time on the  $\tilde{l} = 0$  plane).

Let us first analyze the behavior of the ray transit time considering only meridional rays. Regardless of the type of MSI fiber and the number of layers, the ray transit time always increases as the ray invariant  $\tilde{\beta}$  decreases whenever rays propagate within a certain layer. If rays go beyond the first layer, the ray transit time shows a decrease because rays can now propagate within a less-dense medium in addition to the first layer, which boosts their speed. In each layer, the tendency of the ray transit time is to increase for more tilted rays while they do not pass to the next layer, in which case the ray transit time would decrease again (since  $n_{i+1} < n_i$ ). Regardless of the refractive index profile of the MSI fiber, the minimum transit time ( $t_{\min}$ ) corresponds to rays traveling along the outermost layer with the minimum axial angle ( $\theta_{z_N} = 0$ ) or, equivalently, to rays having  $\tilde{\beta} = n_N$ . The maximum transit time ( $t_{\max}$ ) depends strongly on the fiber refractive index

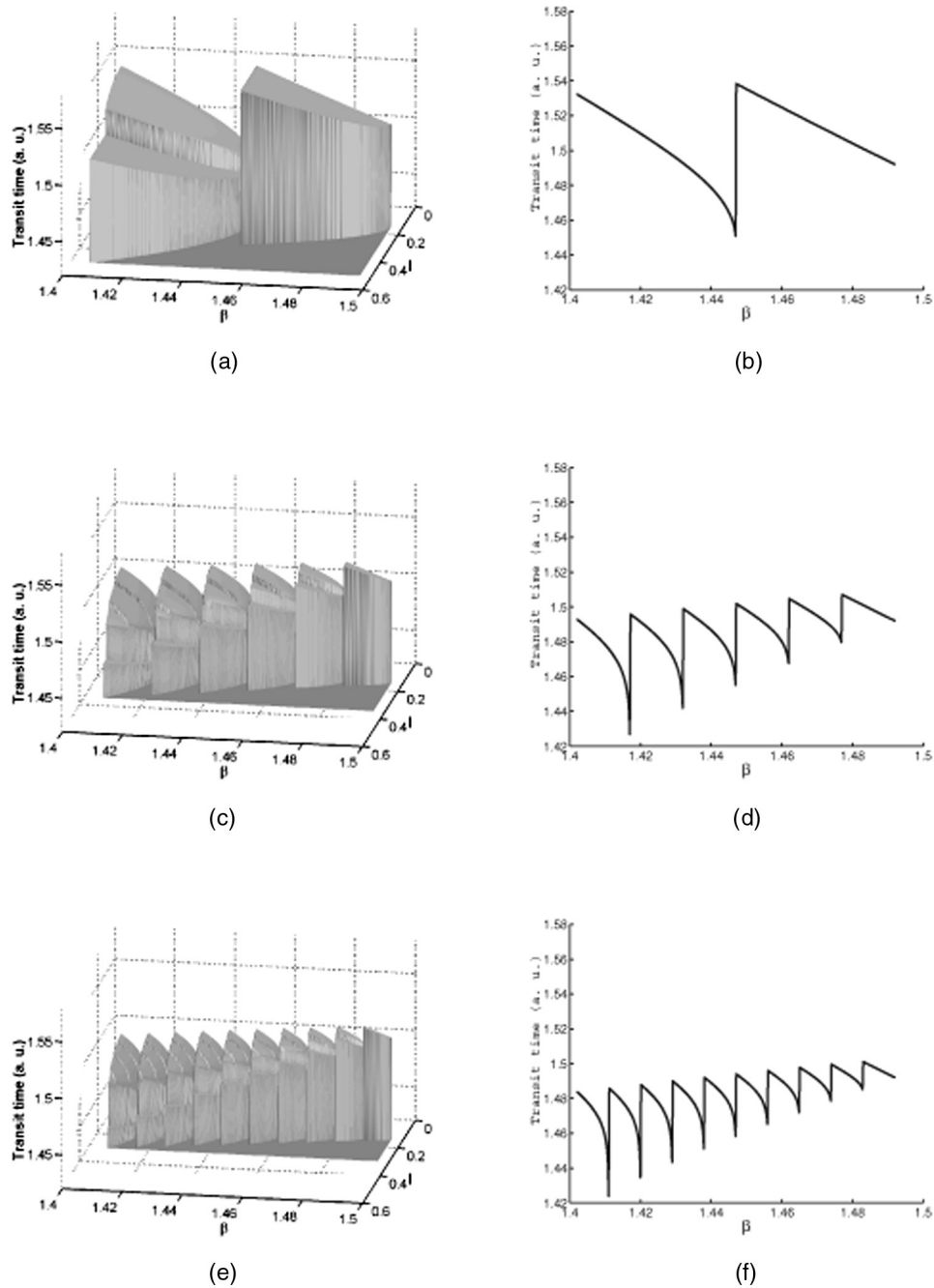
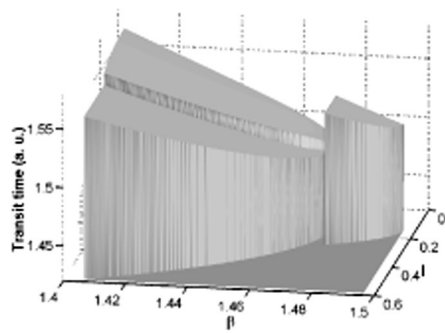
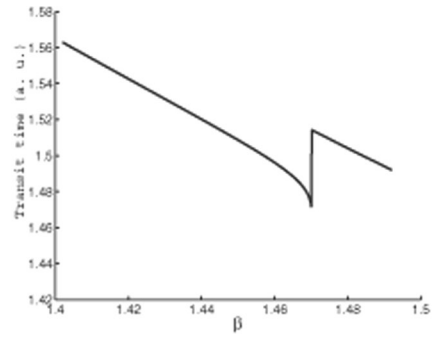


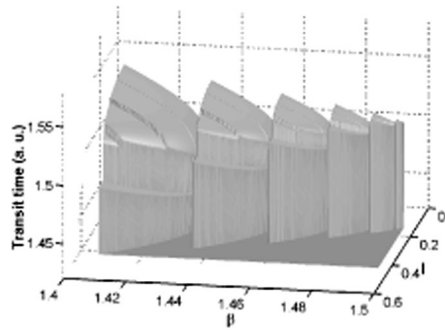
**Figure 9.** Ray transit time for a linear MSI as a function of  $\tilde{\beta}$  and  $\tilde{l}$ : a) two layers; b) two layers (only meridional rays); c) six layers; d) six layers (only meridional rays); e) ten layers; f) ten layers (only meridional rays).



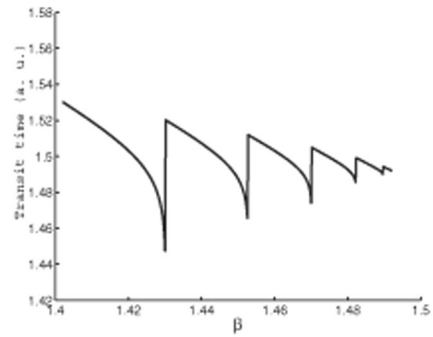
(a)



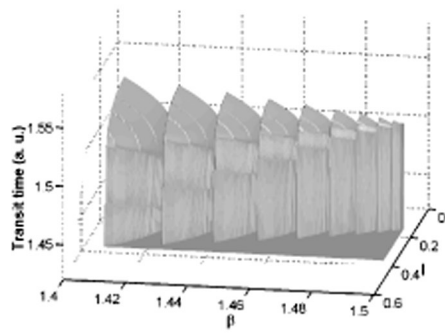
(b)



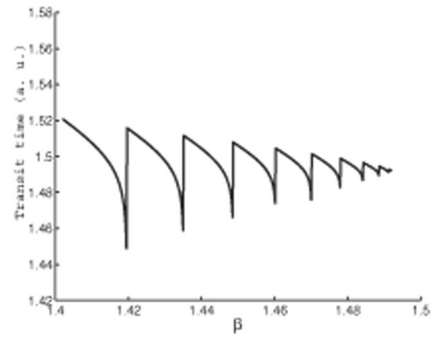
(c)



(d)



(e)



(f)

**Figure 10.** Ray transit time for a parabolic MSI as a function of  $\tilde{\beta}$  and  $\tilde{l}$ : a) two layers; b) two layers (only meridional rays); c) six layers; d) six layers (only meridional rays); e) ten layers; f) ten layers (only meridional rays).

profile. Thus, for a parabolic MSI fiber, the maximum transit time is obtained when rays are tilted at the maximum value allowed for them to propagate as bound rays when they reach the outermost layer. For a linear MSI fiber, the maximum transit time corresponds to rays propagating within the innermost layer and at an angle below the maximum allowed value before they can reach the next layer. This fact can be explained in terms of the difference between refractive indices of consecutive layers. This difference is maximum for the parabolic fit when comparing the refractive indices of the outermost and next to last layers. However, for the linear fit the differences between consecutive layers are the same, so the maximum transit time occurs for the densest medium, which is the innermost one. Even so, the difference between the maximum and minimum transit times tends to decrease as the number of layers increases. The latest topic will also be discussed in the following section.

Turning to the question of the behavior of the ray transit time according to the values of  $\tilde{\beta}$  and  $\tilde{l}$ , it is straightforward to see that it does not depend on  $\tilde{l}$  provided that rays propagate within an only layer, which happens for a ray having a certain  $\tilde{\beta}_{\text{ray}}$  so that  $n_{i+1} \leq \tilde{\beta}_{\text{ray}} < n_i$  (that is, its turning point is  $r_{tp} = \rho_i$ ) and having an  $\tilde{l}$  so that  $\tilde{l}^2 > (n_i^2 - \tilde{\beta}_{\text{ray}}^2)\rho_{i-1}^2/\rho_N^2$  (that is to say, its inner caustic is  $r_{ic} \geq \rho_{i-1}$ ). In contrast, the dependence of the ray transit time on  $\tilde{l}$  is higher as rays propagate within more layers ( $\tilde{\beta}$  decreases) or the number of layers  $N$  increases. Thus, for rays having a certain  $\tilde{\beta}_{\text{ray}}$ ,  $t$  will decrease from a maximum corresponding to  $\tilde{l} = 0$  to a minimum corresponding to the maximum value of  $\tilde{l}$  consistent with Snell's law. The maximum variation of the ray transit time as a function of  $\tilde{l}$  occurs when  $\tilde{\beta} \simeq n_{cl}$  (rays reaching the cladding interface). This maximum variation strongly depends on the number of layers and the fiber refractive index profile.

Although the ray transit time decreases as  $\tilde{l}$  grows, the minimum transit time  $t_{\min}$  corresponds to meridional rays ( $\tilde{l} = 0$ ) reaching the outermost layer of the MSI fiber with a value of  $\tilde{\beta} = n_N$ , irrespective of the refractive index profile of the MSI fiber. Because the ray transit time decreases with  $\tilde{l}$  (when rays propagate within two or more layers), it is clear that the maximum transit time  $t_{\max}$  corresponds to meridional rays, which is obtained under the conditions already discussed.

### Ray Dispersion

Next, we will calculate the pulse spread; that is, the difference between the maximum and minimum ray transit times. As already seen, these maximum and minimum times only depend on  $\tilde{\beta}$ . This fact allows us to discuss the ray dispersion in terms of the expressions obtained for meridional rays, which highly simplifies calculations.

Now, we will calculate  $t_d$  for the case in which there are no skew rays ( $\tilde{l} = 0$ ), that is to say, for meridional rays.

$$t(\tilde{l} = 0) = \begin{cases} \frac{z n_1^2}{c \tilde{\beta}} & \text{when } n_2^2 < \tilde{\beta}^2 < n_1^2 \\ \frac{z}{c \tilde{\beta}} \frac{\frac{n_1^2 \rho_1}{\sqrt{n_1^2 - \tilde{\beta}^2}} + \sum_{i=2}^y \frac{n_i^2}{\sqrt{n_i^2 - \tilde{\beta}^2}} (\rho_i - \rho_{i-1})}{\frac{\rho_1}{\sqrt{n_1^2 - \tilde{\beta}^2}} + \sum_{i=2}^y \frac{\rho_i - \rho_{i-1}}{\sqrt{n_i^2 - \tilde{\beta}^2}}} & \text{when } \begin{cases} n_{y+1}^2 < \tilde{\beta}^2 < n_y^2 \\ y = 2 \dots N \end{cases} \end{cases} \quad (16)$$

The minimum transit time is given by

$$t_{\min} = \frac{z}{c} n_N \quad (17)$$

Evaluating  $t_{\max}$  is a much more complicated task, since

$$\begin{aligned} t_{\max} &= \max\{t_{1\text{st layer}}|\tilde{\beta}=n_2, t_{2\text{nd layer}}|\tilde{\beta}=n_3, \dots, t_{N\text{th layer}}|\tilde{\beta}=n_{cl}\} \\ &= \max\left\{ \frac{z}{c} \frac{n_1^2}{n_2}, \frac{z}{cn_3} \frac{\frac{n_1^2 \rho_1}{\sqrt{n_1^2 - n_3^2}} + \frac{n_2^2}{\sqrt{n_2^2 - n_3^2}} (\rho_2 - \rho_1)}{\frac{\rho_1}{\sqrt{n_1^2 - n_3^2}} + \frac{\rho_2 - \rho_1}{\sqrt{n_2^2 - n_3^2}}}, \dots, \frac{z}{cn_{cl}} \frac{\frac{n_1^2 \rho_1}{\sqrt{n_1^2 - n_{cl}^2}} + \sum_{i=2}^N \frac{n_i^2}{\sqrt{n_i^2 - n_{cl}^2}} (\rho_i - \rho_{i-1})}{\frac{\rho_1}{\sqrt{n_1^2 - n_{cl}^2}} + \sum_{i=2}^N \frac{\rho_i - \rho_{i-1}}{\sqrt{n_i^2 - n_{cl}^2}}} \right\}. \end{aligned} \quad (18)$$

The main advantage of MSI fibers in relation to SI fibers is that now  $t_{\max}$  keeps much lower. However,  $t_{\max} - t_{\min}$  is comparable to the value for SI fibers.

Let us take again the practical case in which the width of each layer is maintained constant ( $\rho_i - \rho_{i-1} = \text{constant } \forall i$ ), whereas we will allow the respective refractive indices to take any value. Now we can simplify Equation (16) so as to have

$$t(\tilde{i} = 0) = \begin{cases} \frac{z}{c} \frac{n_1^2}{\tilde{\beta}} & \text{when } n_2^2 < \tilde{\beta}^2 < n_1^2 \\ \frac{z}{c\tilde{\beta}} \frac{n_1^2 + \left(\frac{\rho_2}{\rho_1} - 1\right) \sqrt{n_1^2 - \tilde{\beta}^2} \sum_{i=2}^y \frac{n_i^2}{\sqrt{n_i^2 - \tilde{\beta}^2}}}{1 + \left(\frac{\rho_2}{\rho_1} - 1\right) \sqrt{n_1^2 - \tilde{\beta}^2} \sum_{i=2}^y \frac{1}{\sqrt{n_i^2 - \tilde{\beta}^2}}} & \text{when } \begin{cases} n_{y+1}^2 < \tilde{\beta}^2 < n_y^2 \\ y = 2 \dots N \end{cases} \end{cases} \quad (19)$$

Now, let us consider the case in which the difference between the refractive indices of the consecutive  $(p-1)$ th and  $p$ th layers is the greatest among the remaining possibilities; that is,

$$n_{p-1} - n_p \gg n_{i-1} - n_i; \quad \begin{matrix} i = 1 \dots N \\ p \neq i \end{matrix}$$

Due to this difference, a greater variation in  $\tilde{\beta}$  is allowed for rays propagating inside the  $p$ th layer. This means that  $t_{\max}$ , evaluated from Equations (18) and (19), is

$$t_{\max} = \frac{z}{cn_p} \frac{n_1^2 + \left(\frac{\rho_2}{\rho_1} - 1\right) \sqrt{n_1^2 - n_p^2} \sum_{i=2}^{p-1} \frac{n_i^2}{\sqrt{n_i^2 - n_p^2}}}{1 + \left(\frac{\rho_2}{\rho_1} - 1\right) \sqrt{n_1^2 - n_p^2} \sum_{i=2}^{p-1} \frac{1}{\sqrt{n_i^2 - n_p^2}}} \quad (20)$$



Hence,  $\Delta t = t_{\max} - t_{\min}$  is calculated from Equations (20) and (17) as

$$\Delta t = \frac{z}{c} \left\{ \frac{n_1^2 + \left(\frac{\rho_2}{\rho_1} - 1\right) \sqrt{n_1^2 - n_p^2} \sum_{i=2}^{p-1} \frac{n_i^2}{\sqrt{n_i^2 - n_p^2}}}{n_p \left[ 1 + \left(\frac{\rho_2}{\rho_1} - 1\right) \sqrt{n_1^2 - n_p^2} \sum_{i=2}^{p-1} \frac{1}{\sqrt{n_i^2 - n_p^2}} \right]} - n_N \right\}. \quad (21)$$

## Fiber Illumination

### Diffuse Illumination

Let us consider a diffuse or Lambertian source. The element of power  $dP$  radiated is given by

$$dP = I(\theta_0) d\Gamma dA$$

where

$$I(\theta_0) = I_0 \cos \theta_0$$

$$d\Gamma = \sin \theta_0 d\theta_0 d\theta_\phi; \quad dA = r dr d\phi$$

and the ranges of source-ray directions ( $\theta_0$  and  $\theta_\phi$ ) and positions on the fiber input endface ( $r$  and  $\phi$ ) satisfy

$$0 \leq \theta_0 \leq \pi/2; \quad 0 \leq r \leq \rho_N,$$

$$0 \leq \theta_\phi \leq 2\pi; \quad 0 \leq \phi \leq 2\pi.$$

The amount of source power carried by bound rays  $P_{br}$  is found by integrating the element of power  $dP$  radiated over the complete ranges of values of  $r$ ,  $\phi$ , and  $\theta_\phi$ , and over the range of values of  $\theta_0$  corresponding to bound rays

$$P_{br} = I_0 \int_0^{2\pi} d\phi \int_0^{\rho_N} r dr \int_0^{2\pi} d\theta_\phi \int_0^{\theta_m(r)} \sin \theta_0 \cos \theta_0 d\theta_0 \quad (22)$$

$\theta_m(r)$  is defined as the maximum value of  $\theta_0$  for which a source ray propagates as a bound ray.

$$n_0 \sin \theta_m(r) = n(r) \sin \theta_c(r) = \begin{cases} n_1 \sin(\theta_{c_1}) = \sqrt{n_1^2 - n_{cl}^2}; & 0 \leq r \leq \rho_1 \\ n_2 \sin(\theta_{c_2}) = \sqrt{n_2^2 - n_{cl}^2}; & \rho_1 \leq r \leq \rho_2 \\ \vdots \\ n_N \sin(\theta_{c_N}) = \sqrt{n_N^2 - n_{cl}^2}; & \rho_{N-1} \leq r \leq \rho_N \end{cases}$$

so that

$$\sin \theta_m(r) = \frac{NA_i}{n_0} = \frac{\sqrt{n_i^2 - n_{cl}^2}}{n_0}; \quad \rho_{i-1} \leq r \leq \rho_i \quad (23)$$

If we substitute  $\theta_m(r)$  for Equation (23) we get the following expression:

$$P_{br} = 2\pi^2 \frac{I_0}{n_0^2} \int_0^{\rho_N} r S(r) dr; \quad S(r) = n_i^2 - n_{cl}^2 = NA_i^2; \quad \rho_{i-1} \leq r \leq \rho_i \quad (24)$$

and this can be expressed as a function of the profile volume  $\Omega$

$$P_{br} = \pi \frac{I_0}{n_0^2} \Omega; \quad \Omega = 2\pi \int_0^{\rho_N} r S(r) dr = 2\pi \int_0^{\rho_N} r (n_i^2 - n_{cl}^2); \quad \rho_{i-1} \leq r \leq \rho_i \quad (25)$$

The above equations can be expanded to obtain

$$\begin{cases} P_{br} = \pi^2 \frac{I_0}{n_0^2} \sum_{i=1}^N (\rho_i^2 - \rho_{i-1}^2) S_i; & S_i = n_i^2 - n_{cl}^2 \\ P_{br} = \pi \frac{I_0}{n_0^2} \Omega; & \Omega = 2\pi \sum_{i=1}^N \frac{\rho_i^2 - \rho_{i-1}^2}{2} (n_i^2 - n_{cl}^2) \end{cases} \quad (\rho_0 = 0) \quad (26)$$

Likewise, the total power  $P_{tot}$  radiated by the source is given by

$$P_{tot} = I_0 \int_0^{2\pi} d\phi \int_0^{\rho_N} r dr \int_0^{2\pi} d\theta_\phi \int_0^{\pi/2} \sin \theta_0 \cos \theta_0 d\theta_0 = \pi^2 \rho_N^2 I_0. \quad (27)$$

Consequently, the source efficiency is

$$\xi = \frac{P_{br}}{P_{tot}} = \frac{P_{br}}{\pi^2 \rho_N^2 I_0} = \frac{\Omega}{n_0^2 \pi \rho_N^2} = \frac{\sum_{i=1}^N (\rho_i^2 - \rho_{i-1}^2) (n_i^2 - n_{cl}^2)}{n_0^2 \rho_N^2} \quad (28)$$

For  $N = 1$ , Equation (28) reduces to the source efficiency for a step-index fiber

$$\xi|_{N=1} = \frac{\rho_1^2 (n_1^2 - n_{cl}^2)}{n_0^2 \rho_1^2} = \frac{n_1^2 - n_{cl}^2}{n_0^2} = \xi_{SI}$$

For the sake of comparison, we also provide the source efficiency for a graded-index fiber, and, more specifically, for a clad power-law profile [31],

$$\xi_{GI} = \frac{q}{q+2} \frac{n_1^2 - n_{cl}^2}{n_0^2}$$

As is stated in Snyder and Love [31], the efficiency for a clad parabolic profile fiber is half of that for a step-index fiber.

Considering again the practical case in which the width of each layer is maintained constant ( $\rho_i - \rho_{i-1} = \text{constant } \forall i$ ), we will calculate the source efficiency for the two different MSI fibers already discussed in the section on ray classification. The results are shown in Figure 11.

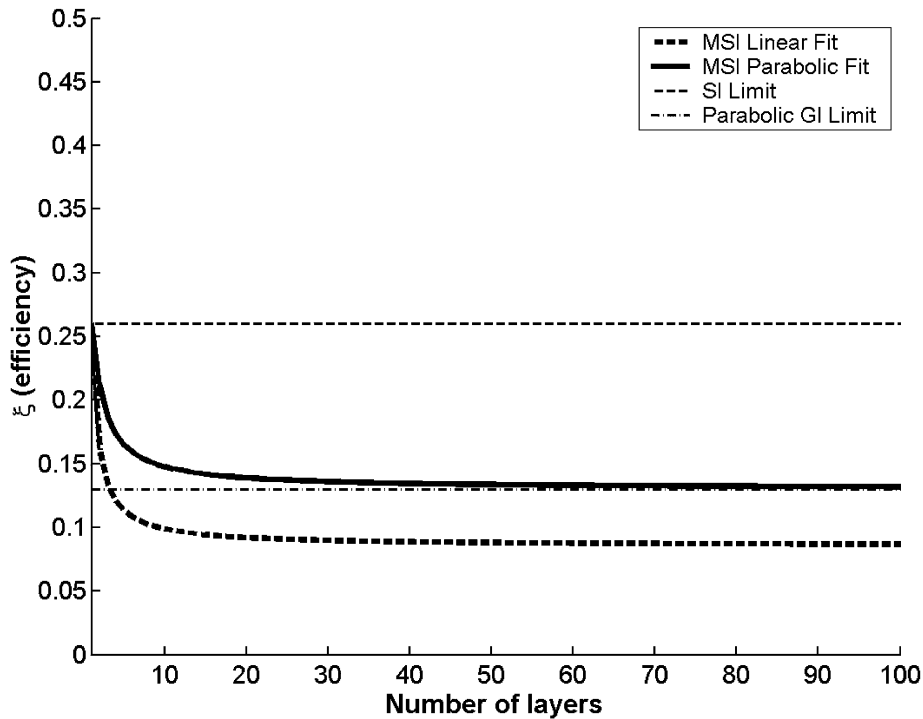


Figure 11. Source efficiency for a diffuse illumination.

The source efficiencies for both MSI fibers match the source efficiency for the step-index fiber in the limit of one layer ( $N = 1$ ). As the number of layers  $N$  increases, the source efficiency for a parabolic MSI fiber (that is, a fiber whose refractive indices are fitted according to the clad parabolic profile) tends to that for a clad parabolic profile fiber. However, the source efficiency for the linear MSI fiber drops below that for a clad parabolic profile fiber, so a linear distribution of the refractive indices for each layer on an MSI fiber leads to a worse power acceptance.

In view of these results, one can compare the source efficiency for an MSI fiber with the source efficiency for a clad power-law profile

$$\frac{q}{q+2} = \frac{\sum_{i=1}^N (\rho_i^2 - \rho_{i-1}^2)(n_i^2 - n_{cl}^2)}{\rho_N^2(n_1^2 - n_{cl}^2)}$$

For a certain MSI fiber, its power acceptance would be the same as that for a clad power-law profile graded-index fiber satisfying

$$q = \frac{2 \sum_{i=1}^N (\rho_i^2 - \rho_{i-1}^2)(n_i^2 - n_{cl}^2)}{\rho_N^2(n_1^2 - n_{cl}^2) - \sum_{i=1}^N (\rho_i^2 - \rho_{i-1}^2)(n_i^2 - n_{cl}^2)} = \frac{2\Omega}{\pi \rho_N^2(n_1^2 - n_{cl}^2) - \Omega}.$$

**Collimated-Beam Illumination**

Let us now consider a collimated-beam illumination emitting at an angle  $\theta_0$  to the fiber axis. If the beam carries uniform power  $P_i$  per unit area of its cross section, then

$$P_{\text{tot}} = \pi \rho_N^2 P_i \cos \theta_0 \quad (29)$$

According to Equation (23), the maximum value of  $\theta_0$  for a source ray to propagate as a bound ray decreases from a maximum value for which

$$\sin \theta_m(r)|_{0 \leq r \leq \rho_1} = \sqrt{n_1^2 - n_{\text{cl}}^2}/n_0$$

to a minimum for which

$$\sin \theta_m(\rho_N) = 0$$

as  $n_i$  decreases from  $n_1$  to  $n_{\text{cl}}$ . Therefore, if

$$\theta_0 > \theta_m(r)|_{0 \leq r \leq \rho_1}$$

that is to say,

$$\theta_0 > \arcsin \left( \sqrt{n_1^2 - n_{\text{cl}}^2}/n_0 \right)$$

no bound rays are excited, but if

$$0 \leq \theta_0 < \theta_m(r)|_{0 \leq r \leq \rho_1}$$

that is,

$$0 \leq \theta_0 < \arcsin \left( \sqrt{n_1^2 - n_{\text{cl}}^2}/n_0 \right)$$

bound rays are excited within a circle whose radius  $r_{br}$  is set by the following condition:

$$r_{br} = \rho_i; \quad \arcsin \left( \sqrt{n_{i+1}^2 - n_{\text{cl}}^2}/n_0 \right) \leq \theta_0 < \arcsin \left( \sqrt{n_i^2 - n_{\text{cl}}^2}/n_0 \right); \quad i = 1 \dots N$$

taking into account that  $n_{N+1} = n_{\text{cl}}$ .

As a consequence, the total bound-ray power and source efficiency are given by

$$P_{br} = \begin{cases} \pi \rho_i^2 P_i; & \arcsin \left( \sqrt{n_{i+1}^2 - n_{\text{cl}}^2}/n_0 \right) \leq \theta_0 < \arcsin \left( \sqrt{n_i^2 - n_{\text{cl}}^2}/n_0 \right) \\ 0; & \arcsin \left( \sqrt{n_1^2 - n_{\text{cl}}^2}/n_0 \right) < \theta_0 \leq \pi/2 \end{cases} \quad (30)$$

$$5\xi = \begin{cases} \frac{\rho_i^2}{\rho_N^2}; & \arcsin \left( \sqrt{n_{i+1}^2 - n_{\text{cl}}^2}/n_0 \right) \leq \theta_0 < \arcsin \left( \sqrt{n_i^2 - n_{\text{cl}}^2}/n_0 \right) \\ 0; & \arcsin \left( \sqrt{n_1^2 - n_{\text{cl}}^2}/n_0 \right) < \theta_0 \leq \pi/2 \end{cases} \quad (31)$$

Again, for  $N = 1$ , Equation (31) reduces to the source efficiency for a step-index fiber

$$\xi|_{N=1} = \xi_{SI} = \begin{cases} 1; & 0 \leq \theta_0 < \theta_m, \\ 0; & \theta_m < \theta_0 \leq \pi/2 \end{cases}$$

where

$$\theta_m = \arcsin\left(\sqrt{n_1^2 - n_{cl}^2}/n_0\right).$$

### Coupling Loss

Mechanical misalignment is a major source of losses when joining two fibers. In this section we will study the first two of three fundamental types of misalignments between fibers, which are, namely, axial or lateral displacement, longitudinal separation, and angular misalignment. The angular misalignment and the measurements of the losses due to these three types of misalignment will be presented in another paper.

#### Lateral Displacement

From Equation (26), we recall the expression for the amount of source power carried by bound rays

$$P_{br} = \pi^2 \frac{I_0}{n_0^2} \sum_{i=1}^N (\rho_i^2 - \rho_{i-1}^2) S_i = \sum_{i=1}^N P_i; \quad S_i = n_i^2 - n_{cl}^2,$$

and taking into account that  $S_i = NA_i^2$ ,

$$P_i = \pi^2 \frac{I_0}{n_0^2} (\rho_i^2 - \rho_{i-1}^2) NA_i^2$$

We can rewrite the above expression as a function of the amount of source power carried by bound rays within the innermost layer,  $P_1$ , so as to have

$$\frac{P_i}{P_1} = \frac{(\rho_i^2 - \rho_{i-1}^2) NA_i^2}{\rho_1^2 NA_1^2}$$

which, in turn, allows us to express the optical power density  $W_i = P_i/A_i$  as a function of the square of the local numerical aperture

$$\frac{W_i}{W_1} = \frac{P_i/A_i}{P_1/A_1} = \frac{[(\rho_i^2 - \rho_{i-1}^2) NA_i^2]/[\pi(\rho_i^2 - \rho_{i-1}^2)]}{[\rho_1^2 NA_1^2]/[\pi\rho_1^2]} = \frac{NA_i^2}{NA_1^2} \quad (32)$$

We will calculate the power transmitted across two fibers joint with an axial offset  $d$ , as shown in Figure 12, by taking into account the areas  $A_{T_1}$  and  $A_{T_2}$  that constitute the overlap region. The power coupled into the receiving fiber is calculated by integrating the power density given by Equation (32) separately over the areas  $A_{T_1}$  and  $A_{T_2}$ . Within  $A_{T_1}$  the local numerical aperture of the emitting fiber is always smaller than that of the layers

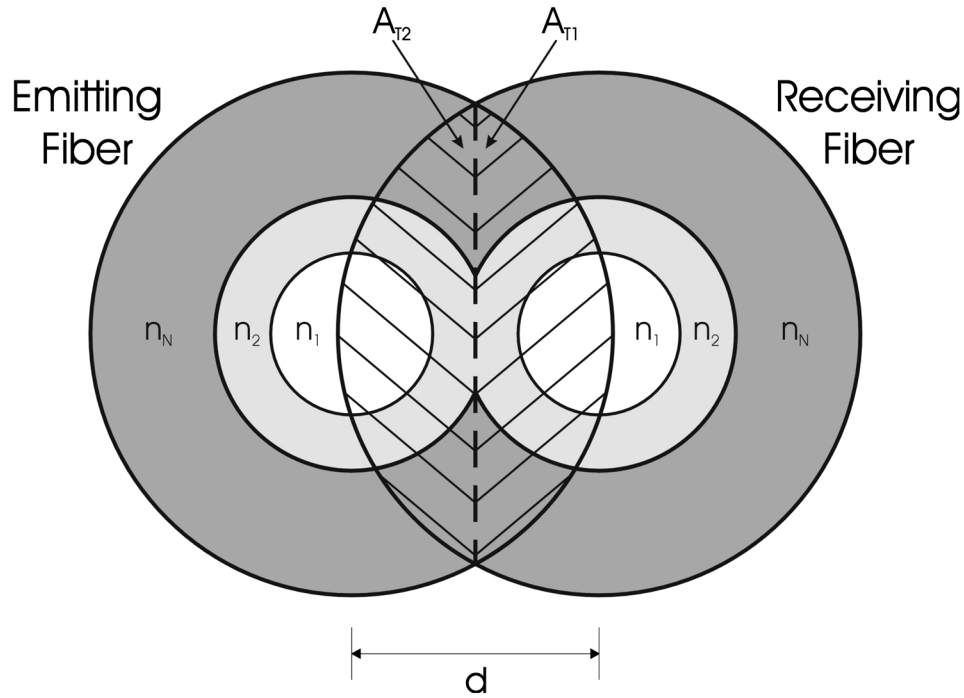


**Figure 12.** Overlapping core areas (stripped areas) for two identical MSI fibers with a lateral misalignment of  $d$ .

of the receiving fiber. Therefore, all the power emitted in this region will be accepted by the receiving fiber, so

$$P_1 = 2 \int_0^{\varphi_N} \int_{r_\varphi}^{\rho_N} W_i r dr d\varphi = 2W_1 \int_0^{\varphi_N} \int_{r_\varphi}^{\rho_N} \frac{NA_i^2}{NA_1^2} r dr d\varphi \quad (33)$$

where the limits of integration are

$$\varphi_N = \arccos \frac{d}{2\rho_N}; \quad r_\varphi = \frac{d}{2 \cos \varphi}$$

$A_{T1}$  can be divided into several sections, each of them corresponding to a different layer. Hence,

$$P_1 = \frac{W_1}{NA_1^2} \left\{ \sum_{i=j+1}^N NA_i^2 A_i + NA_j^2 \left[ \rho_j^2 \arccos \frac{d}{2\rho_j} - \frac{d}{2} \sqrt{\rho_j^2 - d^2/4} \right] \right\} \quad (34)$$

where

$$A_i = \rho_i^2 \arccos \frac{d}{2\rho_i} - \rho_{i-1}^2 \arccos \frac{d}{2\rho_{i-1}} + \frac{d}{2} \left\{ \sqrt{\rho_{i-1}^2 - d^2/4} - \sqrt{\rho_i^2 - d^2/4} \right\}$$

and  $j$  is an integer value that satisfies

$$\rho_{j-1} \leq d/2 < \rho_j$$

Although within  $A_{T_2}$  the local numerical aperture of the emitting fiber can be greater than the local numerical aperture of the receiving fiber, the power  $P_2$  coupled across this area can be readily found from symmetry considerations. Thus, this power  $P_2$  is equal to the power  $P_1$  coupled across the area  $A_{T_1}$  [33], so the total power  $P_{ac}$  accepted by the receiving fiber is

$$P_{ac} = 2P_1 \quad (35)$$

The coupling efficiency  $\eta_{lateral}$  is calculated by dividing this total accepted power  $P_{ac}$  by the total bound-ray power  $P_{br}$

$$\eta_{lateral} = \frac{P_{ac}}{P_{br}} = \frac{\frac{2W_1}{NA_1^2} \left\{ \sum_{i=j+1}^N NA_i^2 A_i + NA_j^2 \left[ \rho_j^2 \arccos \frac{d}{2\rho_j} - \frac{d}{2} \sqrt{\rho_j^2 - d^2/4} \right] \right\}}{\pi^2 \frac{I_0}{n_0^2} \sum_{i=1}^N (\rho_i^2 - \rho_{i-1}^2) NA_i^2} \quad (36)$$

and substituting  $W_1$  for Equation (32) we obtain

$$\eta_{lateral} = \frac{2 \left\{ \sum_{i=j+1}^N NA_i^2 A_i + NA_j^2 \left[ \rho_j^2 \arccos \frac{d}{2\rho_j} - \frac{d}{2} \sqrt{\rho_j^2 - d^2/4} \right] \right\}}{\pi \sum_{i=1}^N (\rho_i^2 - \rho_{i-1}^2) NA_i^2} \quad (37)$$

so the coupling loss for the lateral misalignment  $L_{LM}$  is

$$\begin{aligned} L_{LM} &= -10 \log \eta_{lateral} \\ &= -10 \log \frac{2 \left\{ \sum_{i=j+1}^N NA_i^2 A_i + NA_j^2 \left[ \rho_j^2 \arccos \frac{d}{2\rho_j} - \frac{d}{2} \sqrt{\rho_j^2 - d^2/4} \right] \right\}}{\pi \sum_{i=1}^N (\rho_i^2 - \rho_{i-1}^2) NA_i^2} \end{aligned} \quad (38)$$

It is straightforward to show that for  $N = 1$ , Equation (38) reduces to the coupling loss for a step-index fiber

$$\begin{aligned} L_{LM|N=1} &= -10 \log \frac{2 \left\{ \rho_1^2 \arccos \frac{d}{2\rho_1} - \frac{d}{2} \sqrt{\rho_1^2 - d^2/4} \right\}}{\pi \rho_1^2} \\ &= -10 \log \frac{2}{\pi} \left\{ \arccos \frac{d}{2\rho_1} - \frac{d}{2\rho_1} \sqrt{1 - \left( \frac{d}{2\rho_1} \right)^2} \right\} \end{aligned}$$

Finally, Figure 13 shows the coupling loss for the different types of MSI fibers already discussed in the section on ray classification.

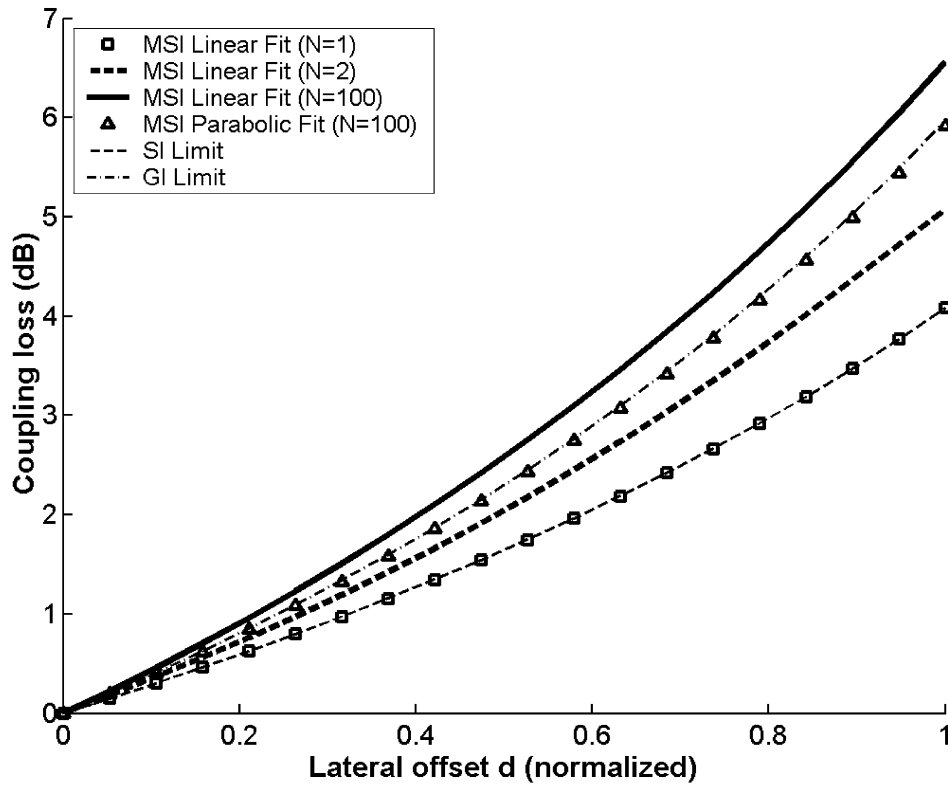


Figure 13. Coupling loss for a lateral misalignment  $d$ .

Again, the coupling loss for an MSI fiber of 1 layer is the same as that for a step-index fiber. As the number of layers  $N$  increases, the coupling loss for an MSI fiber (either linear or parabolic) is greater than the coupling loss for a step-index one. Furthermore, the coupling loss for the parabolic MSI fiber tends to the coupling loss for a clad parabolic profile fiber (as can be seen for  $N = 100$  layers). In contrast, the coupling loss for the linear MSI fiber for  $N = 100$  layers increases beyond the coupling loss for a clad parabolic profile fiber, so a linear distribution of the refractive indices for each layer on an MSI fiber leads to a worse coupling efficiency.

**Longitudinal Separation**

We will analyze the effects of separating the two fiber ends longitudinally by a gap  $s$ . The power into the receiving fiber is calculated from the contribution of each layer of the emitting fiber into each layer of the receiving fiber, taking into account the power acceptance conditions in both fiber ends. For this purpose, each portion of accepted power in the receiving fiber is calculated from the optical power density  $W(r)$ . Assuming a diffuse illumination, at  $z = 0$  the optical power density associated to the  $i$ th layer of the emitting fiber is

$$W_i(0) = \frac{\pi^2 \frac{I_0}{n_0^2} (\rho_i^2 - \rho_{i-1}^2) NA_i^2}{\pi (\rho_i^2 - \rho_{i-1}^2)}$$



whereas at  $z = s$  it is

$$W_i(s) = \frac{\pi^2 \frac{I_0}{n_0^2} (\rho_i^2 - \rho_{i-1}^2) \text{NA}_i^2}{\pi \{(\rho_i + s \tan \theta_i)^2 - (\rho_{i-1} - s \tan \theta_i)^2\}}$$

where

$$\theta_i = \arcsin \frac{\text{NA}_i}{n_0}.$$

We can separate the above expression and have

$$\begin{cases} W_1(s) = \frac{\pi \frac{I_0}{n_0^2} \rho_1^2 \text{NA}_1^2}{(\rho_1 + s \tan \theta_1)^2} \\ W_{i \neq 1}(s) = \frac{\pi I_0}{n_0^2} \frac{\text{NA}_i^2}{\left\{1 + \frac{2s \tan \theta_i}{\rho_i - \rho_{i-1}}\right\}} \end{cases}$$

Likewise, we can classify the accepted power contributions according to whether it is emitted from the innermost layer or not.

- Power contributions of the innermost layer ( $i = 1$ ) of the emitting fiber to the  $j$ th layer of the receiving fiber:

$$P_1^1 = \frac{\pi^2 I_0}{n_0^2} \frac{\text{NA}_1^2}{(\rho_1 + s \tan \theta_1)^2} \rho_1^4 \quad (39)$$

$$P_{j \geq 2}^1 = \frac{\pi^2 I_0}{n_0^2} \frac{\rho_1^2 \text{NA}_j^2}{(\rho_1 + s \tan \theta_1)^2} \{\min[\rho_j^2, (\rho_1 + s \tan \theta_1)^2] - \rho_{j-1}^2\} \quad (40)$$

- Power contributions of the rest of the layers ( $i \geq 2$ ) of the emitting fiber to the  $j$ th layer of the receiving fiber:

$$P_1^{i \geq 2} = \frac{\pi^2 I_0}{n_0^2} \frac{\text{NA}_i^2}{\left\{1 + \frac{2s \tan \theta_i}{\rho_i - \rho_{i-1}}\right\}} [\rho_1^2 - (\rho_{i-1} - s \tan \theta_i)^2] \quad (41)$$

$$P_{j \geq 2}^{i \geq 2} = \begin{cases} \frac{\pi^2 I_0}{n_0^2} \frac{\text{NA}_j^2}{\left\{1 + \frac{2s \tan \theta_j}{\rho_j - \rho_{j-1}}\right\}} \left\{ \begin{aligned} &\min[\rho_j^2, (\rho_i + s \tan \theta_i)^2] \\ &- \max[\rho_{j-1}^2, (\rho_{i-1} - s \tan \theta_i)^2] \end{aligned} \right\} & \text{if } i < j \\ \frac{\pi^2 I_0}{n_0^2} \frac{\text{NA}_i^2}{\left\{1 + \frac{2s \tan \theta_i}{\rho_i - \rho_{i-1}}\right\}} \left\{ \begin{aligned} &\min[\rho_j^2, (\rho_i + s \tan \theta_i)^2] \\ &- \max[\rho_{j-1}^2, (\rho_{i-1} - s \tan \theta_i)^2] \end{aligned} \right\} & \text{if } i \geq j \end{cases} \quad (42)$$

Therefore,

$$P_{ac} = P_1^1 + \sum_{i=2}^p P_1^i + \sum_{j=2}^q P_j^1 + \sum_{j=2}^N \sum_{i=s}^t P_j^i \tag{43}$$

where the limits of integration  $p, q, s,$  and  $t$  are integer values satisfying

$$p = \max \{ \text{all possible values of } k \} \text{ so that } \rho_{k-1} - s \tan \theta_k < \rho_1; \quad p = 2 \dots N$$

$$q = \max \{ \text{all possible values of } k \} \text{ so that } \rho_{k-1} \leq \rho_1 + s \tan \theta_1 < \rho_k; \quad q = 2 \dots N$$

$$s = \min \{ \text{all possible values of } k \} \text{ so that } (\rho_k + s \tan \theta_k \geq \rho_{j-1}) \text{ and } (\rho_{k-1} - s \tan \theta_k < \rho_j)$$

$$t = \max \{ \text{all possible values of } k \} \text{ so that } (\rho_k + s \tan \theta_k \geq \rho_{j-1}) \text{ and } (\rho_{k-1} - s \tan \theta_k < \rho_j); \quad 2 \leq s \leq t \leq N$$

and Equation (43) is only valid for

$$s \leq \frac{\rho_1}{\tan \theta_2}$$

so a uniform optical power density can still be assumed.

We have plotted on Figure 14 the coupling loss for the different types of MSI fibers considered in the section on ray classification.

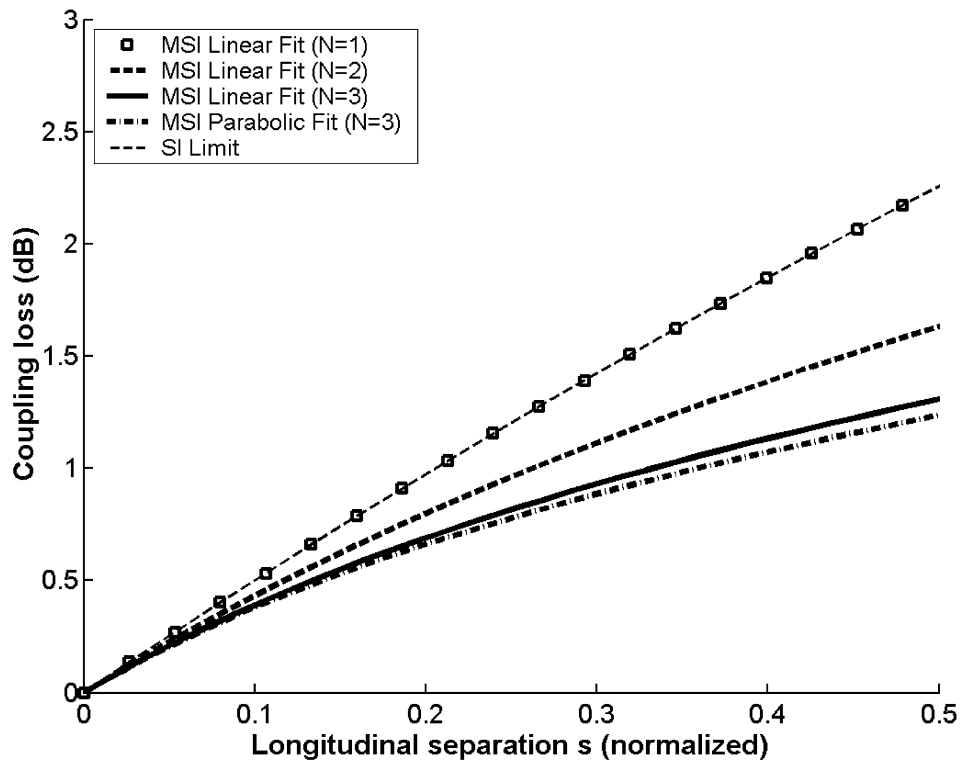


Figure 14. Coupling loss for a longitudinal separation  $s$ .

As could be expected, the coupling loss for an MSI fiber of one layer is the same as that for a step-index fiber. Contrary to what occurred to the coupling loss due to a lateral displacement, as the number  $N$  of layers increases, the coupling loss for an MSI fiber (either linear or parabolic) is less than the coupling loss for a step-index one. In addition, the difference between the coupling loss for the parabolic MSI fiber and that for the linear MSI fiber is not very significant. Even so, the former is slightly smaller than the latter, so a linear distribution of the refractive indices for each layer on an MSI fiber leads to a worse coupling efficiency, in the same way as in lateral displacements.

## Conclusion

POFs' characteristics, namely price, ease of connection, and good physical properties, make them specially suitable for short-haul telecommunication links and sensors, which has motivated us to work on this field. In this article we have summarized some of the results obtained, both from measurements and prototypes and from theoretical investigations. These include propagation studies, simulation of real fibers, and the design of new components for POFs and sensors based on them.

In the second part of the article we have presented a new theory for MSI-POF based on geometric optics, which could be a serious alternative to GI-POF, as the results obtained for ray dispersion seem to confirm. The geometric optics approach will be completed at a further stage by analyzing bend losses and power redistribution, and by performing empirical measurements, in order to ensure the validity of the expressions we have calculated.

## References

1. Zubia, J., and J. Arrue. 2001. Plastic optical fibers: An introduction to their technological processes and applications. *Opt. Fiber Technol.* 7:101.
2. Naritomi, M. 1996. CYTOP<sup>®</sup> amorphous fluoropolymers for low loss POF. POF Asia Pacific Forum 1996, December, Tokyo, Japan.
3. Koike, Y., T. Ishigure, and E. Nihei. 1995. High-bandwidth graded index polymer optical fiber. *J. Lightwave Technol.* 13:1475.
4. Ishigure, T., E. Nihei, and Y. Koike. 1996. Optimum refractive index profile for graded-index polymer optical fibres, toward gigabit data links. *Appl. Opt.* 35(12):2048.
5. Bluoss, E., J. Vinogradov, and O. Ziemann. 2002. World record distance for video transmission on standard PMMA-POF. Proceedings of the Eleventh International Conference on Plastic Optical Fibres and Applications—POF'2002, 131, September 18–20, 2002, Tokyo, Japan.
6. Khoe, G. D., T. Koonen, I. Tafur, H. Boom, P. Bennekom, and A. Ng'oma. 2002. High capacity polymer optical fibre systems. Proceedings of the Eleventh International Conference on Plastic Optical Fibres and Applications—POF'2002, 3, September 18–20, 2002, Tokyo, Japan.
7. Levin, V., T. Baskakova, Z. Lavrova, A. Zubkov, H. Poisel, and K. Klein. 1999. Production of multilayer polymer optical fibers. Proceedings of the Conference POF'1999, 98, July 14–16, 1999, Chiba, Japan.
8. Irie, K., Y. Uozu, and T. Yoshimura. 2001. Structure design and analysis of broadband POF. Proceedings of the Conference POF'2001, 73, September 27–30, 2001, Amsterdam, The Netherlands.
9. Arrue, J., and J. Zubia. 1994. Components choice to lengthen low speed plastic fiber optical communications links. Proceedings of the Third International Conference on Plastic Optical Fibres and Applications—POF'94, 78, October 26–28, 1994, Yokohama, Japan.
10. Arrue, J., and J. Zubia. 1996. Analysis of the decrease in attenuation by properly bending plastic optical fibres. *IEE Proceedings—Optoelectronics*, 143(2):135.

11. Maruo, S., M. Kawase, and J. Yoshida. 2000. Mode mixing experiments on high NA POFs. Proceedings of the Ninth International Conference on Plastic Optical Fibers and Applications, September 5–8, 2000, Boston, MA.
12. Arrue, J., J. Zubia, G. Durana, and J. Mateo. 2001. Parameters affecting bending losses in graded-index polymer optical fibers. *IEEE J. Selected Topics Quantum Electron.* 17(5):836.
13. Durana, G., J. Zubia, J. Arrue, and G. Aldabaldetrek. 2003. Dependence of bending losses on cladding thickness in plastic optical fibers. *Appl. Opt.* 42(6):997.
14. Zubia, J., and J. Arrue. 1997. Theoretical analysis of the torsion induced optical effect in a plastic optical fiber. *Opt. Fiber Technol.* 3:162.
15. Zubia, J., and J. Arrue. 1997. Theoretical analysis of the modal dispersion induced by stresses in a multimode plastic optical fiber. *IEEE Proc. Optoelectron.* 144(6):397.
16. Zubia, J., G. Durana, J. Arrue, I. Garces, and M. Lopez-Amo. 2001. Polarimetry of plastic optical fibers. Proceedings of the International Symposium on Photonic Systems and Applications SPIE'2001, Singapore.
17. Zubia, J., G. Durana, G. Aldabaldetrek, J. Arrue, M. A. Losada, and M. Lopez-Higuera. 2003. New method to calculate mode conversion coefficients in SI multimode optical fibers. *IEEE J. Lightwave Technol.* 21(3):776.
18. Losada, M. A., I. Garces, J. Mateo, I. Salinas, J. Lou, and J. Zubia. 2002. Mode coupling contribution to radiation losses in curvatures for high and low numerical aperture plastic optical fibers. *IEEE J. Lightwave Technol.* 20(7):1160.
19. Zubia, J., H. Poisel, C.-A. Bunge, G. Aldabaldetrek, and J. Arrue. 2002. POF modelling. Proceedings of the Eleventh International Conference on Plastic Optical Fibers and Applications, September 18–20, 2002, Tokyo, Japan.
20. Arrue, J., J. Zubia, G. Fuster, and D. Kalymnios. 1997. Theoretical understanding of experimental results on bent plastic optical fibers. Proceedings of the Sixth International Conference on Plastic Optical Fibers and Applications, September 22–25, 1997, Kauai, Hawaii.
21. Arrue, J., J. Zubia, G. Fuster, and D. Kalymnios. 1998. Light power behaviour when bending plastic optical fibers. *IEE Proc. Optoelectron.* 145(6):313.
22. Arrue, J., J. Zubia, N. Merino, and D. Kalymnios. 2000. Bending losses in graded index fibers. Proceedings of the Ninth International Conference on Plastic Optical Fibers and Applications, September 5–8, 2000, Boston, MA.
23. Arrue, J., J. Zubia, G. Durana, J. Mateo, and M. Lopez-Amo. 2001. Model for the propagation of pulses and mode scrambling in a real POF with structural imperfections. Proceedings of the Tenth International Conference on Plastic Optical Fibers and Applications, Amsterdam, The Netherlands.
24. Arrue, J., J. Zubia, G. Durana, G. Aldabaldetrek, and M. Lopez-Amo. 2002. Analysis of the parameters affecting the design and operation of a scrambler for graded-index POF, on the basis of a standard configuration. Proceedings of the Eleventh International Conference on Plastic Optical Fibers and Applications, September 18–20, 2002, Tokyo, Japan.
25. Aguirre, A., U. Irusta, J. Zubia, and J. Arrue. 1997. Fabrication of low loss POF contact couplers. Proceedings of the Sixth International Conference on Plastic Optical Fibers and Applications, Kauai, Hawaii.
26. Zubia, J., U. Irusta, and J. Arrue. 1998. Design and characterization of a plastic optical fiber active coupler. *IEEE Photonics Technol. Lett.* 10(11):1578.
27. Zubia, J., G. Durana, J. Arrue, and I. Garces. 2002. Design and performance of a new active coupler for plastic optical fibers. *Electron. Lett.* 38(2):65.
28. Zubia, J., O. Aresti, J. Arrue, J. Miskowicz, and M. Lopez-Amo. 2000. Barrier sensor based on plastic optical fibers to determine the wind speed at a wind generator. *IEEE J. Selected Topics Quantum Electron.* 6(5):773.
29. Lomer, M., J. Etxebarria, J. Zubia, and J. M. Lopez-Higuera. 2000. In situ measurement of hydrofluoric and hydrochloric acid concentrations using POF. Proceedings of the Ninth International Conference on Plastic Optical Fibers and Applications—POF'00, 164, September 5–8, 2000, Boston, MA.

30. Zubia, J., G. Garitaonandia, and J. Arrue. 2000. Passive device based on plastic optical fiber to determine the index of refraction of liquids. *Appl. Opt.* 39(6):941.
31. Snyder, A. W., and J. D. Love. 1983. *Optical waveguide theory*. London: Chapman and Hall.
32. Eska Miu, Mitsubishi Rayon Co. Ltd. Available: <http://www.pofeska.com>
33. Keiser, G. 1991. *Optical fiber communications*. McGraw-Hill.

## Biographies

**J. Zubia** received a degree in solid-state physics in 1988 and a Ph.D. in physics from the University of the Basque Country in 1993. His Ph.D. work focused on optical properties of ferroelectric liquid crystals. He is a full professor at the Telecommunications Engineering School (University of the Basque Country, Bilbao, Spain). He has more than ten years of experience doing basic research in the field of plastic optical fibers. At present, he is involved in research projects in collaboration with universities and companies from Spain and other countries in the field of plastic optical fibers, fiber-optic sensors, and liquid crystals. Professor Zubia won a special award for best thesis in 1995.

**G. Aldabaldetrek** holds an MSc degree in telecommunications engineering and is currently pursuing a Ph.D. in telecommunications engineering at the Telecommunications Engineering School (University of the Basque Country, Bilbao, Spain). Since 2002 he has been a lecturer at the Telecommunications Engineering School of the University of the Basque Country in Bilbao, Spain.

**G. Durana** received a degree in solid-state physics in 1999 from the University of the Basque Country and he is currently pursuing a Ph.D. in telecommunications engineering at the Telecommunications Engineering School (University of the Basque Country, Bilbao, Spain). Since 2001 he has been a lecturer at the Telecommunications Engineering School of the University of the Basque Country in Bilbao, Spain.

**J. Arrue** received a B.S. in electronic physics, an M.S. in electronics and telecommunications, and Ph.D. in optical fibers from the University of the Basque Country. He is a professor at the Telecommunications Engineering School (University of the Basque Country, Bilbao, Spain). He has been involved in international research projects for ten years.

**C.-A. Bunge** received a diploma in electrical engineering in 1999 and a Ph.D. from the Technical University of Berlin in 2003. He studied the propagation and attenuation properties of POF and of multimode fibers. Since 2002 he has been with the POF-AC of the University of Applied Sciences in Nuremberg, Germany, as scientific director and is responsible for international projects. His current scientific work deals with modeling of all kinds of POFs, especially multi step-index POF and the newly developed M-POF.

**H. Poisel** is professor at the University of Applied Sciences Nuremberg. He earned his diploma in physics in 1977 and his Ph.D. in physics of the Technical University Munich in 1983. He worked as a researcher and project manager for IABG and MBB, both of Ottobrunn, Germany, until he joined the University of Applied Sciences in 1991. Since 2000 he is the director of the POF-AC. His scientific works include studies on fiber-optic sensors, especially fiber-optic gyro, and optical properties of Polymer Optical Fibers. Currently he deals with applications of POF for illumination, sensors, and data transmission.